

~~CONFIDENTIAL~~

Copy 227
RM L50G07

NACA RM L50G07

7200

0143803



TECH LIBRARY KAFB, NM

NACA

RESEARCH MEMORANDUM

LANGLEY 9-INCH SUPERSONIC TUNNEL TESTS OF SEVERAL
MODIFICATIONS OF A SUPERSONIC MISSILE HAVING TANDEM
CRUCIFORM LIFTING SURFACES

THREE-COMPONENT DATA RESULTS OF MODELS HAVING RATIOS
OF WING SPAN TO TAIL SPAN EQUAL TO AND LESS THAN 1 AND
SOME STATIC ROLLING-MOMENT DATA

By Robert W. Rainey

Langley Aeronautical Laboratory
Langley Field, Va.

CLASSIFIED DOCUMENT

This document contains classified information affecting the National Defense of the United States within the meaning of the Espionage Act, USC 50:31 and 32. Its transmission or the revelation of its contents in any manner to an unauthorized person is prohibited by law.
Information so classified may be imparted only to persons in the military and naval services of the United States, appropriate civilian officers and employees of the Federal Government who have a legitimate interest therein, and to United States citizens of known loyalty and discretion who of necessity must be informed thereof.

**NATIONAL ADVISORY COMMITTEE
FOR AERONAUTICS**

WASHINGTON
March 7, 1951

~~CONFIDENTIAL~~

CLASSIFICATION OF THIS DOCUMENT IS Unclassified

By authority of NASA Tech Rep Announcement #R 7...
(OFFICER AUTHORIZED TO CHANGE)

By 1 Sept. 68

..... MK

GRADE OF OFFICER MAKING CHANGE)

14 Feb. 61
DATE

1
NACA RM L50G07[REDACTED]
NATIONAL ADVISORY COMMITTEE FOR AERONAUTICS

RESEARCH MEMORANDUM

LANGLEY 9-INCH SUPERSONIC TUNNEL TESTS OF SEVERAL
MODIFICATIONS OF A SUPERSONIC MISSILE HAVING TANDEM
CRUCIFORM LIFTING SURFACESTHREE-COMPONENT DATA RESULTS OF MODELS HAVING RATIOS
OF WING SPAN TO TAIL SPAN EQUAL TO AND LESS THAN 1 AND
SOME STATIC ROLLING-MOMENT DATA

By Robert W. Rainey

SUMMARY

Lift, drag, and pitching-moment data and some static rolling-moment data are presented for missile configurations having wing-tail-span ratios equal to and less than 1. These configurations included variations in wing and tail plan forms, wing-tail-span ratios, body length, and nose shape. Also, data from tests of elements and various combinations of elements of the missile configurations, made to permit an evaluation of the interference effects, are presented. These data were obtained in the Langley 9-inch supersonic tunnel and cover an angle-of-attack range from -5° to 15° and a Mach number range from 1.62 to 2.40. Most of the data, however, were obtained at a Mach number of 1.93. The Reynolds number at a Mach number of 1.93 was 0.27×10^6 based on the maximum body diameter. The data show the effects of wing-tail interference on the static longitudinal stability of these missile configurations.

INTRODUCTION

In reference 1, the first paper of a series of three papers, are presented the lift, drag, and pitching-moment characteristics of a "basic" missile having wing-tail-span ratios equal to 1 and several

[REDACTED]

modified versions of the basic missile. These modifications included changes in body length, interdigitation angle, and wing plan form.

In the present paper, the second of the series, are presented three-component measurements and some static rolling-moment measurements of several modified versions of the basic missile. These modifications included changes in wing and tail plan forms of configurations having wing-tail-span ratio equal to 1 and less than 1 as well as changes in interdigitation angle, nose shape, and body length. Also included are results of breakdown or component tests of the various elements and combinations of elements of the modified missiles.

Of special interest are the results of tests of configurations having ring tails and a rectangular tail with moderate aspect ratio. These configurations as well as all the configurations having wing-tail-span ratios less than 1 were devised as a means of placing a portion of the rear surfaces outside of the region of high resultant downwash produced by the wings. Also of special interest are the results of tests of configurations using the same tail surfaces but having systematic variations made in the wing-tail-span ratios while maintaining the same wing plan form.

All tests were made in the Mach number range of 1.62 to 2.40 at corresponding Reynolds numbers from 0.362×10^6 to 0.262×10^6 per inch. With the data obtained in these tests it is possible to obtain the characteristics of one component in the presence of another or others. In order to expedite publication of these data, no analyses of results are presented.

To be presented in a subsequent paper are the results of tests of four more modified versions of the original missile, these modified versions having wing-tail-span ratios less than 1.

SYMBOLS

S	maximum body cross-sectional area
d	maximum body diameter
C_l	rolling-moment coefficient $\left(\frac{\text{Rolling moment}}{qSd} \right)$
C_L	lift coefficient $\left(\frac{\text{Lift}}{qS} \right)$

C_m pitching-moment coefficient, moments taken about center of gravity, see figure 1 $\left(\frac{\text{Pitching moment}}{qSd} \right)$

$$C_{m\alpha} = \frac{\partial C_m}{\partial \alpha}$$

C_D drag coefficient $\left(\frac{\text{Drag}}{qS} \right)$

q dynamic pressure $\left(\frac{\rho V^2}{2} \right)$

α angle of attack, degrees

ϕ angle of roll of model relative to angle-of-attack plane, positive when model, viewed from rear, is rotated clockwise ($\phi = 0^\circ$ when opposite tail panels are in angle-of-attack plane)

θ angle between a plane through opposite tail panels and a plane through opposite wing panels, positive when wings are rotated clockwise with respect to tails, when the model is viewed from rear. The angle θ is always less than 90° , and its value appears as the superscript for W in the model configuration designations. When θ values (superscripts on W) are indicated for BW configurations, the subtracted tail is assumed to be present at $\theta = 0^\circ$.

B configuration of body

BT configuration of body and tails

BW configuration of body and wings

BWT configuration of body, wings, and tails

Subscripts:

1 to 9 refers to the particular body, wing, or tail plan form (see fig. 1)

R wing panels reversed so that leading edge becomes trailing edge

T body has internal taper at stern

Superscript:

Numerical superscript for W gives value of θ (See definition of θ).

APPARATUS AND TEST PROCEDURE

Wind Tunnel

All tests were conducted in the Langley 9-inch supersonic tunnel which is a continuous-operation closed-circuit type in which the stream pressure, temperature, and humidity conditions can be controlled and regulated. Different test Mach numbers are provided by interchanging nozzle blocks which form test sections approximately 9 inches square. Throughout the present tests, the moisture content in the tunnel was kept sufficiently low so that the effects of condensation in the supersonic nozzle were negligible. Eleven fine-mesh turbulence-damping screens are provided in the relatively large area settling chamber just ahead of the supersonic nozzle. A schlieren optical system is provided for qualitative visual flow observations.

Test Setup and Models

A schematic drawing of the model installation in the tunnel is shown in reference 1 with a description of the test setup. For the present tests requiring rolling-moment data, a strain-gage balance was installed inside the model and replaced part of the spindle.

Dimensions and designations of the various models used in the present tests are given in figure 1 with the exception of W_2 which was defined in reference 1. Two W_4 wings were tested, one with constant thickness and rounded leading edge (designated "rounded leading edge"), the other with thickness taper and sharp leading edge (designated "sharp leading edge"). The plan forms were identical within the tolerances of construction. Models were found generally to be accurate within ± 0.002 inch of the dimensions shown. The various wings and tails of the various configurations could be changed, located differently with respect to each other on the body, reversed, or omitted entirely. Body lengths could be changed by inserting sections in the cylindrical portion. Also, nose shapes could be changed by a simple interchange of parts. All the elements and combinations of elements of the models reported in the present paper are in the index of figures. All models tested had an internal taper at the stern of the body and the elevators soldered fixed to the tail panels. Some body-alone tests

were made by use of "solid" models having surfaces that were free of waviness and perturbations; these tests are discussed in the section entitled "Presentation of Data."

PRECISION OF DATA

For all the test Mach numbers, pressure surveys throughout the test section have shown the stream to be uniform within a maximum variation in Mach number of ± 0.01 . Less detailed angle surveys have indicated negligible flow deviations, and, also from past experience, both zero moment and zero lift are generally realized for symmetrical configurations at zero angle of attack. These points are brought out to emphasize the fact that for the present tests when an unexpected moment or lift appears at zero angle of attack, several possibilities exist; namely, the configuration is asymmetrical, the flow about the symmetrical configuration is asymmetrical, and/or an extraneous force appears as a result of the flow around the support system or windshield. For the present tests, the most likely reason for an extraneous moment or lift at zero angle of attack is a misaligned (other than zero angle with respect to the body axis) wing or tail panel. Measurements of the various wings and tails indicated that inadvertent incidences are present which contributed to the various lifts and moments evident at zero angle of attack.

All the lift, drag, and pitching moment were measured by means of self-balancing mechanical scales. A conservative estimate of the maximum probable errors in these measurements is given in the following table:

Mach number \ Coefficient	1.62	1.93	2.40
C_L	± 0.001	± 0.001	± 0.001
C_D	± 0.003	± 0.003	± 0.004
C_m	± 0.013	± 0.014	± 0.020

The rolling moments were measured by use of a strain-gage balance installed inside of the model during the tests requiring such data. The maximum design rolling moment for the balance was 0.50 inch-pound. It was found that individual test points were repeatable to within ± 0.002 inch-pound or a C_l of about ± 0.001 . Corrections were made for

the interaction of lift upon rolling moment; however, the effects of side force were not correctable since the side forces were not known. An estimate of the contribution to rolling moment by side force was found to be small, a maximum of 0.015 inch-pound for a body-wing-tail combination at such a roll angle as to realize large side forces at angles of attack. In summarizing this discussion, it may be concluded that the maximum possible errors in the measured rolling-moment coefficients are ± 0.001 for configurations where side forces are absent and from ± 0.001 to ± 0.007 for configurations where side forces are realized, the exact value depending upon the amount of side force present.

Reference to the data will show that these errors in the forces and moments are probably very small as compared with the scatter about a mean curve or displacement of a mean curve arising from other errors.

Angles of attack with respect to each other in a given run are accurate to within $\pm 0.01^\circ$. The errors in initially referencing the body axis parallel to the air stream may be up to 0.03° .

PRESENTATION OF DATA

The lift, drag, and pitching-moment data are presented in figures 2 to 36, and the rolling-moment data, in figures 37 to 39. An index precedes the figures in which the figures are listed in order of presentation. The figures are grouped according to Mach number, and for each Mach number, the data are approximately in the order of the model buildup, that is, first body alone, then body and wing, and so forth. Included in the present paper are results of tests of three configurations with the forward lifting surfaces reversed, and those configurations are indicated by a subscript R to the wing designation (see figs. 14, 18, and 34). In the case of $B_{4T}W_{2R}^{45T}_1$, the reversed wing W_{2R} was located so that the centroid of its plan form was at about the same longitudinal station as the centroid of the plan form of W_1 in the configuration $B_{4T}W_1^{45T}_1$, and the leading edge of W_{2R} intersected the body 5.25 inches rearward of the nose of the missile.

Body-Alone Tests

It was noted in some cases that for repeat tests of body-alone configurations the pitching-moment coefficients were not in good

agreement above an angle of attack of 9° . It was suspected that a slightly misaligned body section might be sufficient to alter the flow about the body, thereby changing the measured characteristics. Therefore, a solid model of B_{2T} , relatively free of surface irregularities, was tested (test 52 - run 76). A repeat test of B_{2T} using the "sectional" body was then made after using extreme care in alining the body sections (test 52 - run 77A). A third test of B_{2T} was made after intentionally misaligning the body section just rearward of the nose about 0.0005 inch (test 52 - run 77B). The results (see fig. 24) indicated that the pitching-moment data for the solid model and the carefully alined "sectional" model are in good agreement throughout the angle-of-attack range tested. The effect on the pitching-moment data of misaligning the body section was to alter the data at angles of attack greater than 9° in the direction of that for B_{2T} with transition induced by a transition strip (test 50 - run 25, fig. 24). In view of these results, solid models of B_{3T} and B_{4T} were constructed and have been tested at a Mach number of 1.93 (see figs. 2, 3, and 4).

These observations indicated that the boundary layer over the surface of the body was laminar and that transition might be readily induced by small protuberances as mentioned previously in reference 1. Larger "protuberances," such as wings, were expected to induce transition; therefore, tests of B_{2T} , B_{3T} , and B_{4T} were made with transition induced by transition rings installed in the region where the various wings were installed. Each ring was composed of fine salt crystals sparsely distributed in a single layer over a width of about 1/8 inch and a thickness of about 0.013 inch (1.6 percent diameter). The results of these tests are indicated in figures 3, 4, 24, and 35 and are compared with the clean-body tests. In the cases of B_{3T} and B_{4T} , for which transition was induced at three longitudinal stations, it was noted that the decrease in $C_{m\alpha}$ at an angle of attack of about 8° was progressively less as transition was induced farther forward on the bodies. Progressive increments of drag increase as associated with the increased length of turbulent boundary layer were also indicated.

Ring-Tail Tests

Another interesting result of the tests that appears significant was the effect of the ring tails, T_2 and T_3 , upon the pitching-moment

characteristics of the complete missile. The ring tail was devised as a means of placing a portion of the rear surfaces outside of the trailing vortex sheets produced by the wings without increasing the span of the tail. As a means of rapidly assessing its possibilities, a ring with not-too-sharp edges was placed around the tips of T_1 and designated as T_2 . The tail T_3 consisted of a ring supported by "struts" having about the same geometry as the elevators of T_1 (see fig. 1). To compare the results of T_2 and T_3 with T_1 the references of the pitching-moment calculations were moved rearward on all models utilizing T_2 and T_3 (see fig. 1) so that $C_{m\alpha}$ at $\alpha = 0^\circ$ for $B_{2T_1} W_1^{45T_2}$ and $B_{2T_1} W_1^{45T_3}$ was about the same as for $B_{2T_1} W_1^{45T_1}$ (see figs. 30 and 31). As indicated by these data, the use of T_2 or T_3 with either in-line or interdigitated missile configuration resulted in smaller changes in $C_{m\alpha}$, and consequently smaller changes in center-of-pressure travel, below $\alpha = 12^\circ$ than were evident with the use of T_1 (compare figs. 30 and 31 and figs. 28 and 32). The large changes in $C_{m\alpha}$ noted above $\alpha = 12^\circ$ were caused by a loss in tail loading as the upper portion of the ring passed through the trailing vortex systems behind the wings.

Rectangular-Tail Tests

Another means by which the characteristic variations in $C_{m\alpha}$ were decreased was by use of a rectangular tail T_6 , the span of which was equal to the diagonal of the square formed by the wings; that is, the tail span was $\sqrt{2}$ times the wing span (see fig. 1). This tail was in effect a medium-aspect-ratio tail (aspect ratio of 5) behind a low-aspect-ratio wing (aspect ratio of 1.32). Here again, throughout the angle-of-attack range tested, a portion of the tail was believed to have been outside of the body-wing downwash field, and no large variations in $C_{m\alpha}$ were evident for the configurations tested (compare fig. 15 with figs. 13 and 17).

Systematic Tests with Varying Wing-Tail-Span Ratios

In order to obtain experimental data to assess and develop means for calculating wing-body and wing-tail interference, systematic tests were made of configurations with varying wing-tail-span ratios. The data from these tests are presented in figures 8, 21, 22, and 23. These data were from tests of configurations having wings of triangular plan form in which the wing-tail-span ratios were varied systematically. The values of wing-tail-span ratio and the corresponding configuration

designations were 0.618 ($B_{4T}W_7^{\theta T_5}$), 0.745 ($B_{4T}W_8^{\theta T_5}$), and 0.872 ($B_{4T}W_9^{\theta T_5}$) with the trailing edge of each wing located at the same longitudinal station (see fig. 1). These data indicated that regardless of configuration the variations of $C_{m\alpha}$ with α were small. For the in-line BWT configurations, as the wing span became smaller, $C_{m\alpha}$ at $\alpha = 0^\circ$ became progressively more negative and the change in $C_{m\alpha}$ with α became progressively smaller. For the interdigitated BWT configurations, $C_{m\alpha}$ at $\alpha = 0^\circ$ also became progressively more negative as the wing span became smaller, although not so noticeably as did the in-line BWT configurations. Likewise, the changes in $C_{m\alpha}$ with α were less than for the in-line configurations. For in-line and interdigitated configurations, as the wing became smaller, the data approached that of the BT configuration (infinitely small wing).

Other data which are presented in order to assess wing-tail interference were from tests of $B_{4T}W_5^{\theta T_5}$ and $B_{4T}W_6^{\theta T_5}$. For these tests, wings of similar plan form and wing-tail-span ratios of 0.618 ($B_{4T}W_5^{\theta T_5}$) and 0.69 ($B_{4T}W_6^{\theta T_5}$) were utilized, each wing at a different longitudinal station (see fig. 1). These data are presented in figures 7, 19, and 20. Here again the variations of $C_{m\alpha}$ with α were small. The configuration $B_{4T}W_5^{\theta T_5}$ (forward wing) resulted in a more negative C_m slope at $\alpha = 0^\circ$ and less change in $C_{m\alpha}$ as α increased as compared with

~~CONFIDENTIAL~~

$B_{4T}W_6^0T_5$. For the interdigitated cases, $C_{m\alpha}$ at $\alpha = 0^\circ$ was about the same for both BWT configurations with the change in $C_{m\alpha}$ with α being slightly greater for $B_{4T}W_5^{45}T_5$.

Langley Aeronautical Laboratory
National Advisory Committee for Aeronautics
Langley Field, Va.

REFERENCE

1. Rainey, Robert W.: Langley 9-Inch Supersonic Tunnel Tests of Several Modifications of a Supersonic Missile Having Tandem Cruciform Lifting Surfaces. Three-Component Data Results of Models Having Ratios of Wing Span to Tail Span Equal to 1. NACA RM L9L30, 1951.

~~CONFIDENTIAL~~

INDEX OF FIGURES

Figure	Mach number	Figure legends
1	--	Model dimensions and center-of-gravity location
2	1.93	Basic solid and sectional body characteristics, B_{2T} Basic solid and sectional body characteristics, B_{4T}
3	1.93	Effects of transition on basic body characteristics, B_{3T}
4	1.93	Effects of transition on basic body characteristics, B_{4T}
5	1.93	W_1^{45} increments on B_{2T} at roll angles
6	1.93	W_{1R}^0 increments on B_{2T} W_{1R}^{45} increments on B_{2T} W_4^{45} increments on B_{4T} W_{1A}^{45} increments on B_{4T} at roll angles
7	1.93	W_5^0 increments on B_{4T} at roll angles W_6^0 increments on B_{4T} at roll angles
8	1.93	W_7^0 increments on B_{4T} at roll angles W_8^0 increments on B_{4T} at roll angles W_9^0 increments on B_{4T} at roll angles
9	1.93	T_1 increments on B_{2T} at roll angles T_4 increments on B_{4T} at roll angles
10	1.93	T_5 increments on B_{4T} at roll angles T_6 increments on B_{2T} at roll angles

INDEX OF FIGURES - Continued

Figure	Mach number	Figure legends
11	1.93	$B_{2T}W_1^0T_1$ at roll angles
12	1.93	$B_{2T}W_1^{30}T_1$ at roll angles
13	1.93	$B_{2T}W_1^{45}T_1$ at roll angles
14	1.93	$B_{2T}W_{1R}^0T_1$ at roll angles $B_{2T}W_{1R}^{45}T_1$ at roll angles $B_{3T}W_1^{45}T_1$
15	1.93	$B_{2T}W_1^{45}T_6$ at roll angles $B_{4T}W_{1A}^{45}T_6$ $B_{4T}W_{1A}^0T_6$
16	1.93	$B_{4T}W_1^{45}T_1$ at roll angles
17	1.93	$B_{4T}W_{1A}^{45}T_4$ at roll angles $B_{4T}W_{1A}^0T_4$ at roll angles
18	1.93	$B_{4T}W_{2R}^{45}T_1$ Effect of wing leading-edge shape and thickness distribution on $B_{4T}W_4^{45}T_1$
19	1.93	$B_{4T}W_5^{45}T_5$ at roll angles $B_{4T}W_5^0T_5$ at roll angles
20	1.93	$B_{4T}W_6^{45}T_5$ at roll angles $B_{4T}W_6^0T_5$ at roll angles

CONFIDENTIAL

INDEX OF FIGURES - Continued

Figure	Mach number	Figure legends
21	1.93	$B_{4T}W_7^{45T_5}$ at roll angles $B_{4T}W_7^{0T_5}$ at roll angles
22	1.93	$B_{4T}W_8^{45T_5}$ at roll angles $B_{4T}W_8^{0T_5}$ at roll angles
23	1.93	$B_{4T}W_9^{45T_5}$ at roll angles $B_{4T}W_9^{0T_5}$ at roll angles
24	1.62	Basic sectional and solid body characteristics, B_{2T} Effects of transition and misaligned body section on B_{2T} Basic sectional body characteristics, B_{4T}
25	1.62	W_1^{45} increments on B_{2T} at roll angles
26	1.62	T_1 increments on B_{2T} at roll angles
27	1.62	T_2 increments on B_{2T} at roll angles T_3 increments on B_{2T} at roll angles
28	1.62	$B_{2T}W_1^{0T_1}$ at roll angles
29	1.62	$B_{2T}W_1^{30T_1}$ at roll angles
30	1.62	$B_{2T}W_1^{45T_1}$ at roll angles
31	1.62	$B_{2T}W_1^{45T_2}$ at roll angles $B_{2T}W_1^{45T_3}$ at roll angles

INDEX OF FIGURES - Concluded

Figure	Mach number	Figure legends
32	1.62	$B_{2T}W_1^{0T_2}$ at roll angles $B_{2T}W_1^{0T_3}$ at roll angles
33	1.62	$B_{4T}W_1^{45T_1}$ at roll angles
34	1.62	$B_{4T}W_{2R}^{45T_1}$ $B_{4T}W_4^{45T_1}$ (with sharp leading edge)
35	2.40	Effects of transition on basic body characteristics, B_{2T} Basic body characteristics, B_{4T} W_1^{45} increments on B_{4T}
36	2.40	$B_{4T}W_1^{45T_1}$ at roll angles
37	1.93	Rolling-moment characteristics of various configurations
38	1.62	Rolling-moment characteristics of various configurations
39	2.40	Rolling-moment characteristics of various configurations

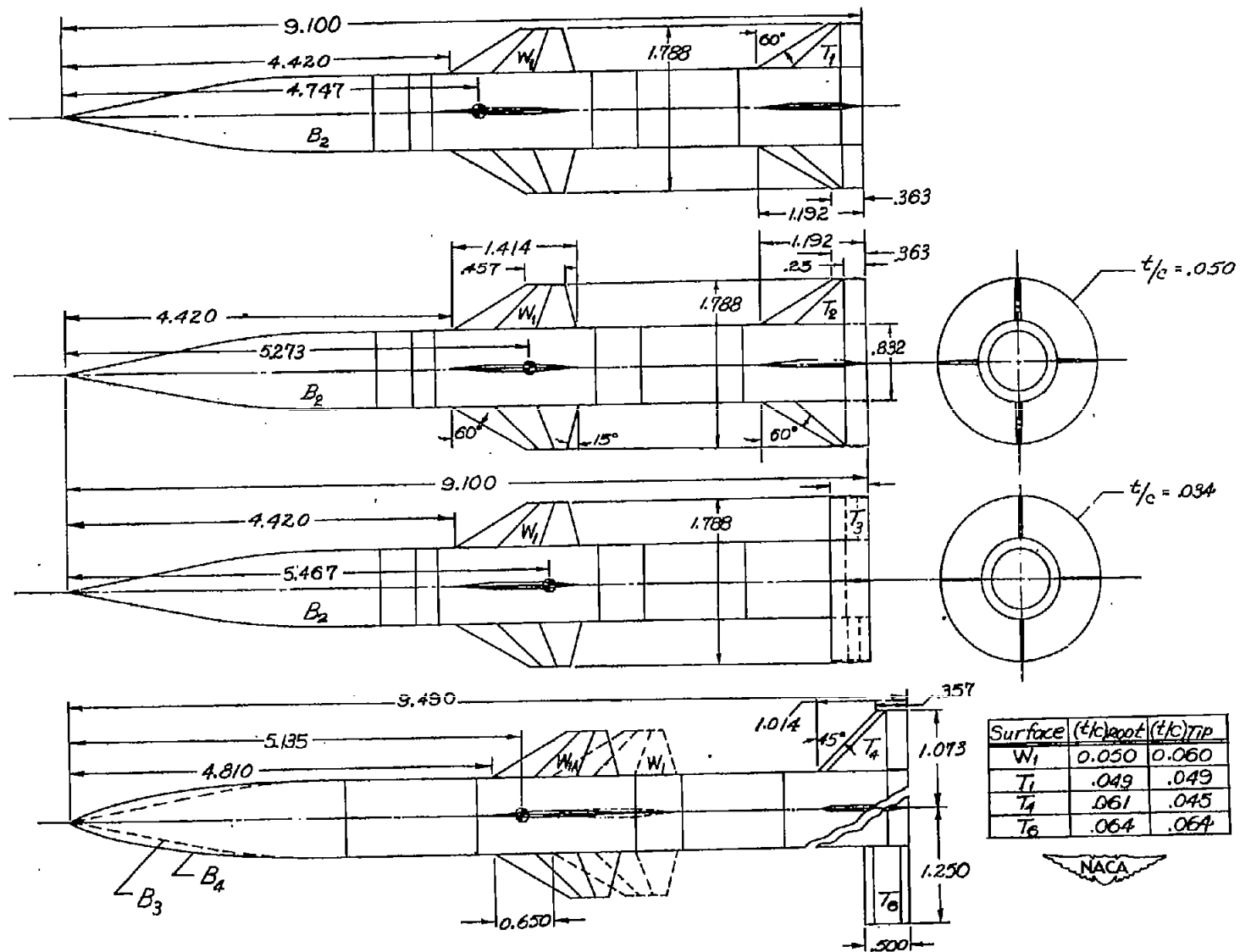


Figure 1.- Model dimensions and center-of-gravity location.

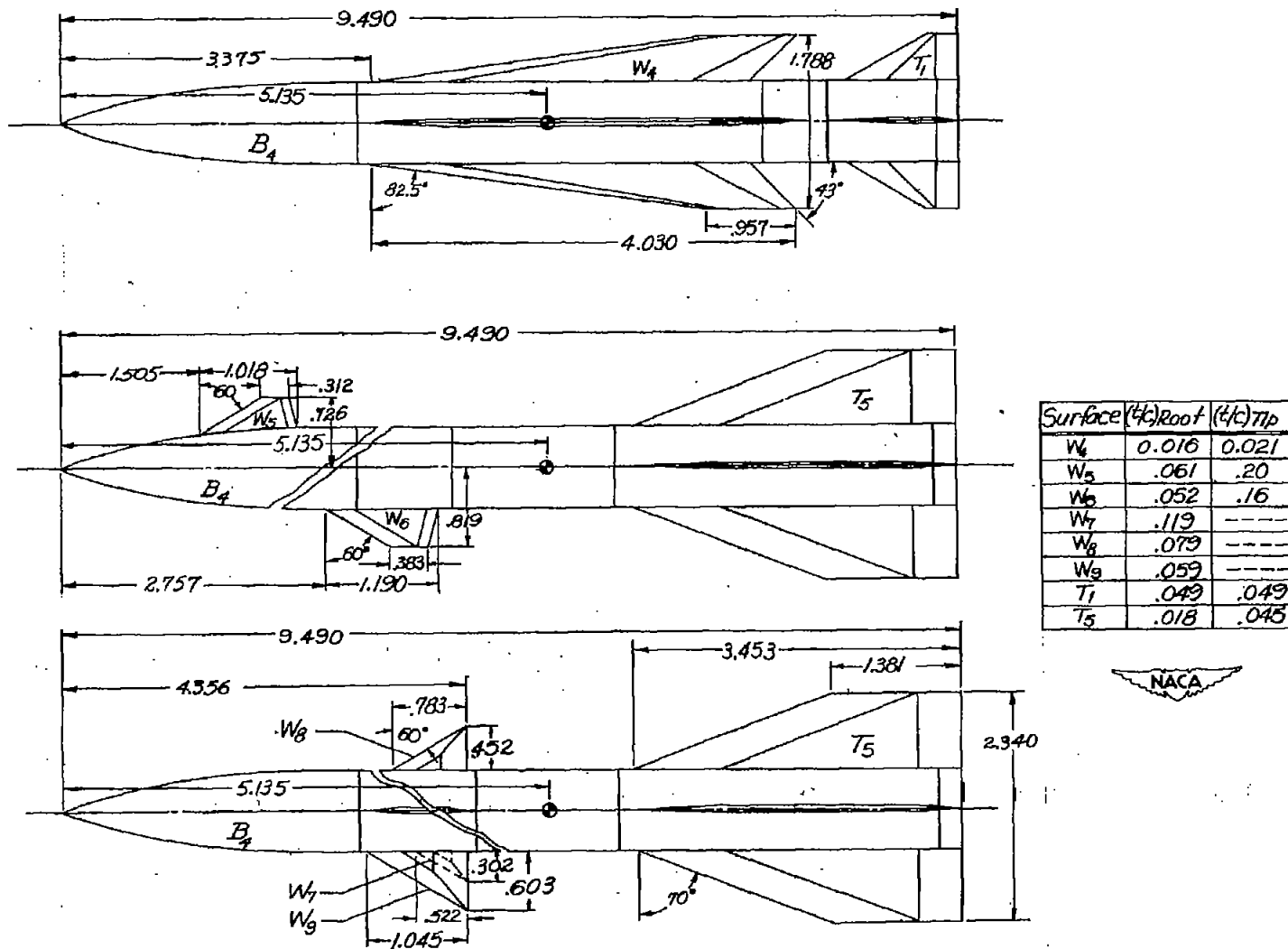


Figure 1.- Concluded.

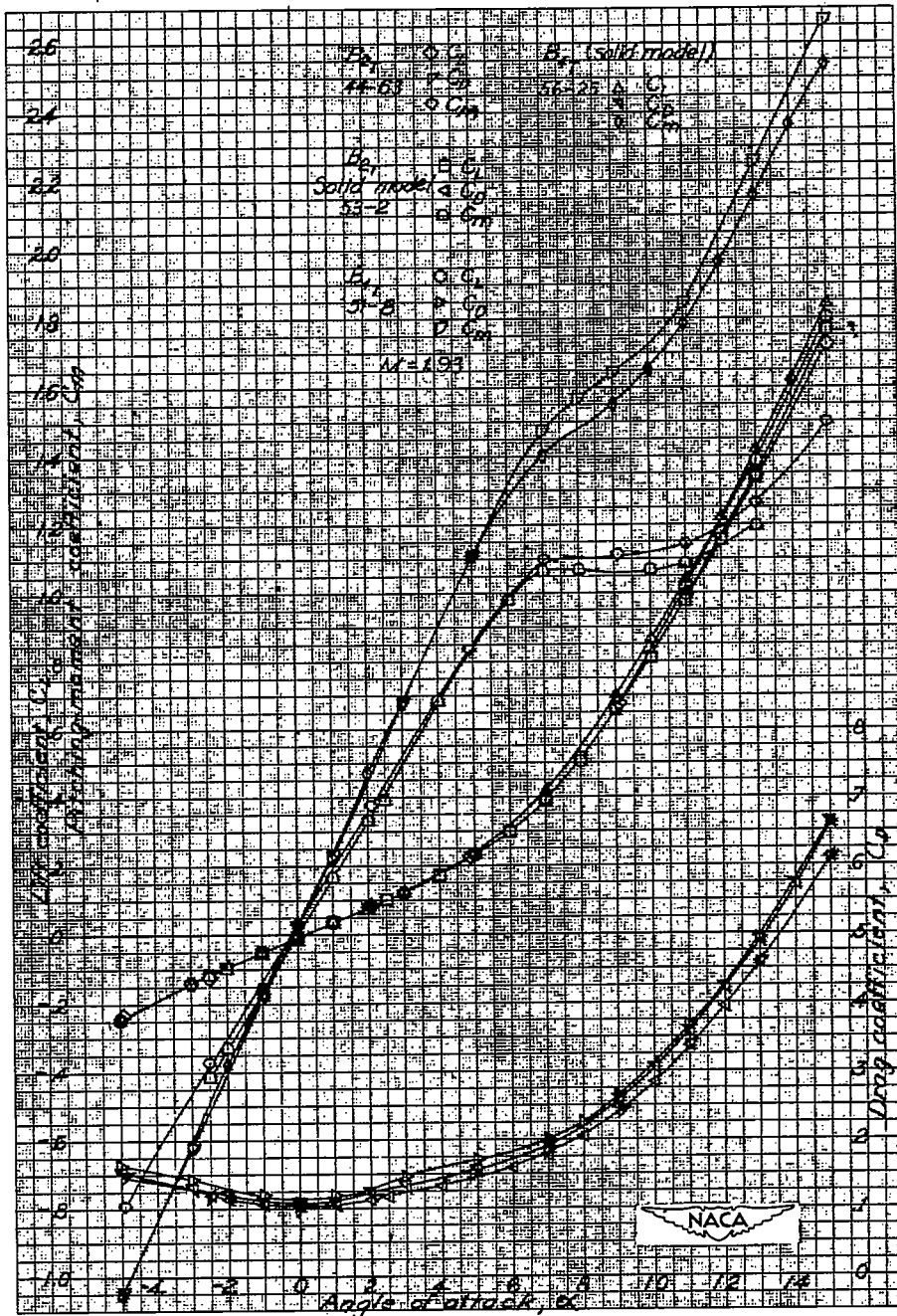


Figure 2.- M = 1.93: Basic solid and sectional body characteristics, B_{2T} and B_{1TP} .

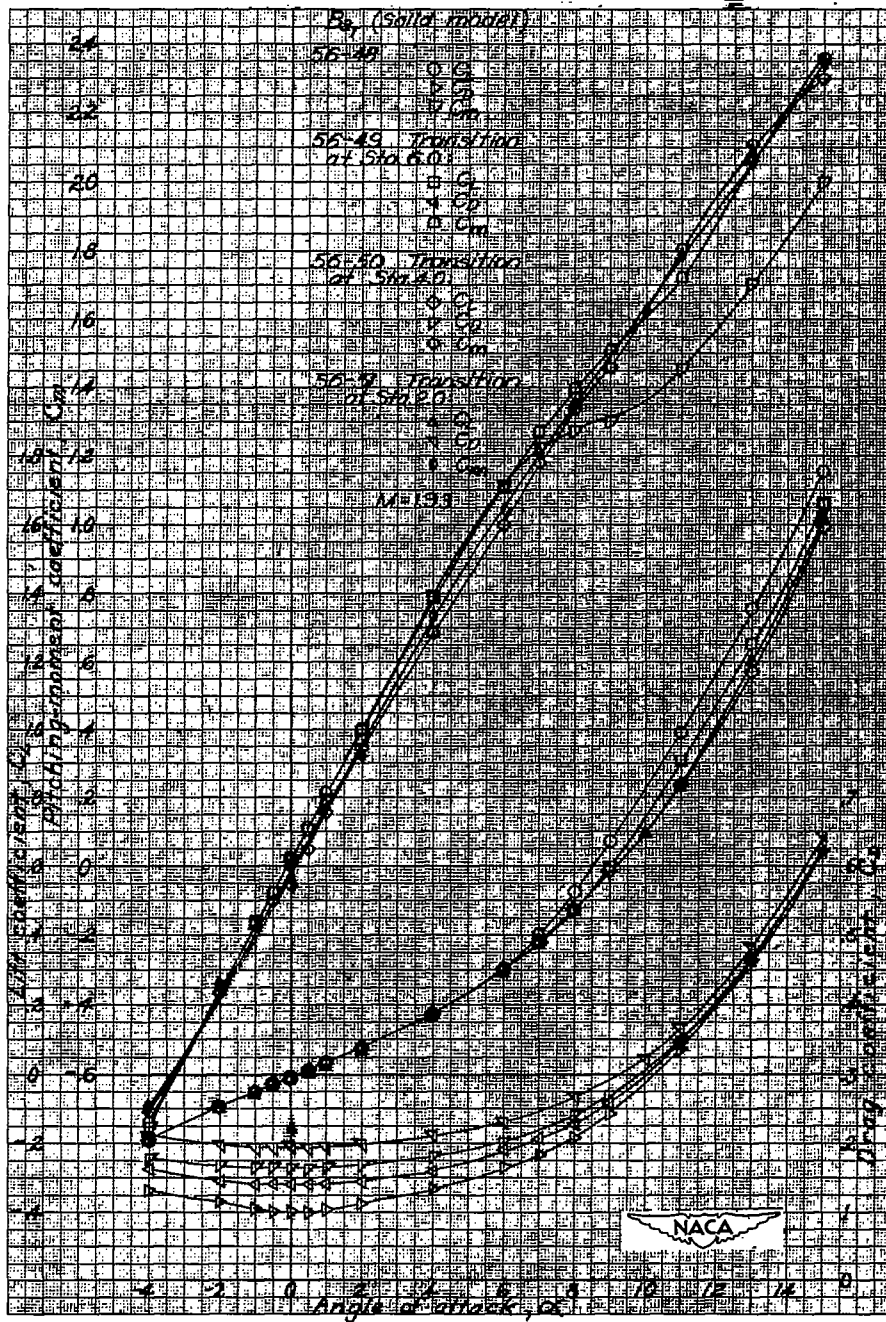


Figure 3.- $M = 1.93$: Effects of transition on basic body characteristics, $B_{3\pi}$.

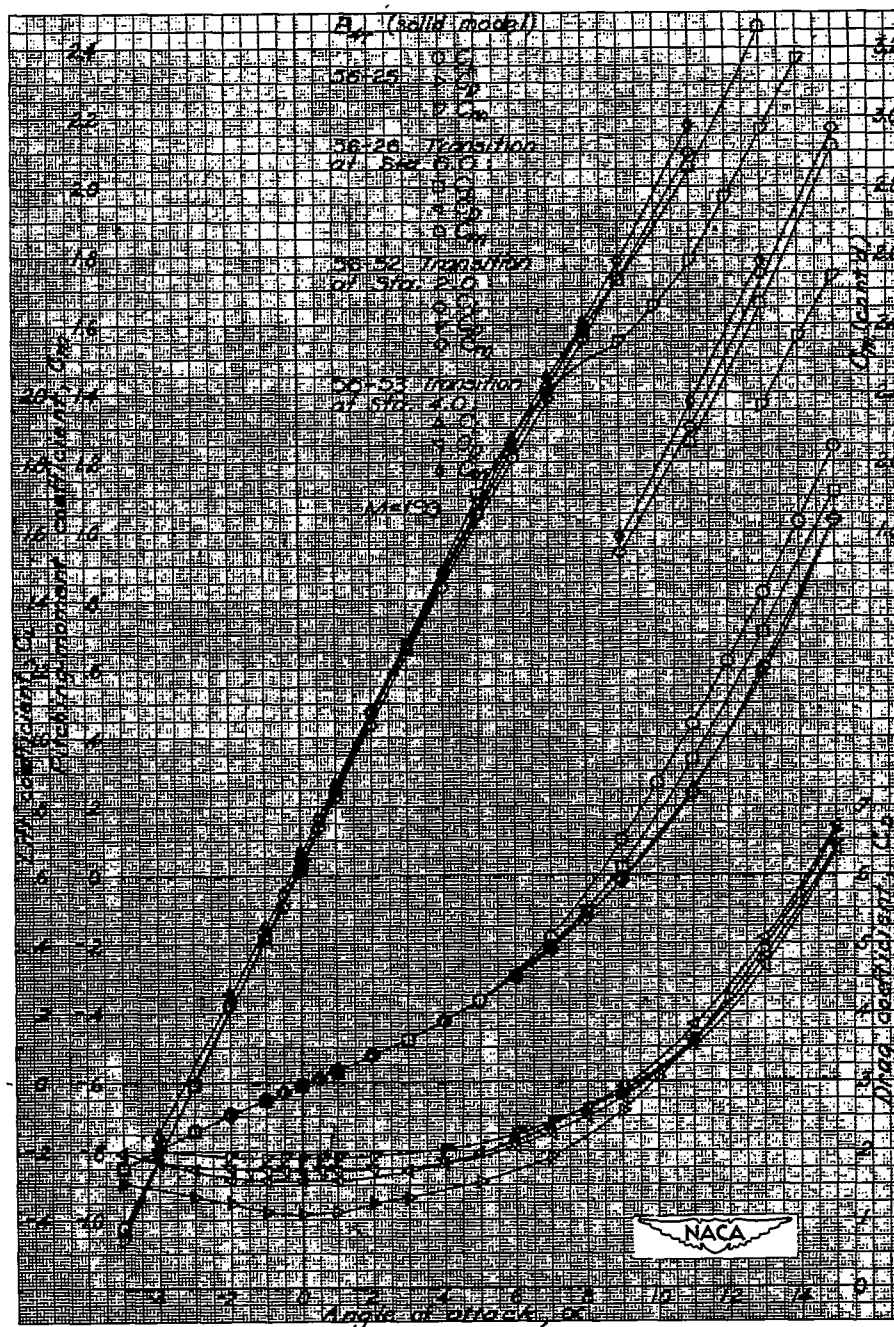


Figure 4.- $M = 1.93$: Effects of transition on basic body characteristics, B_{4T} .

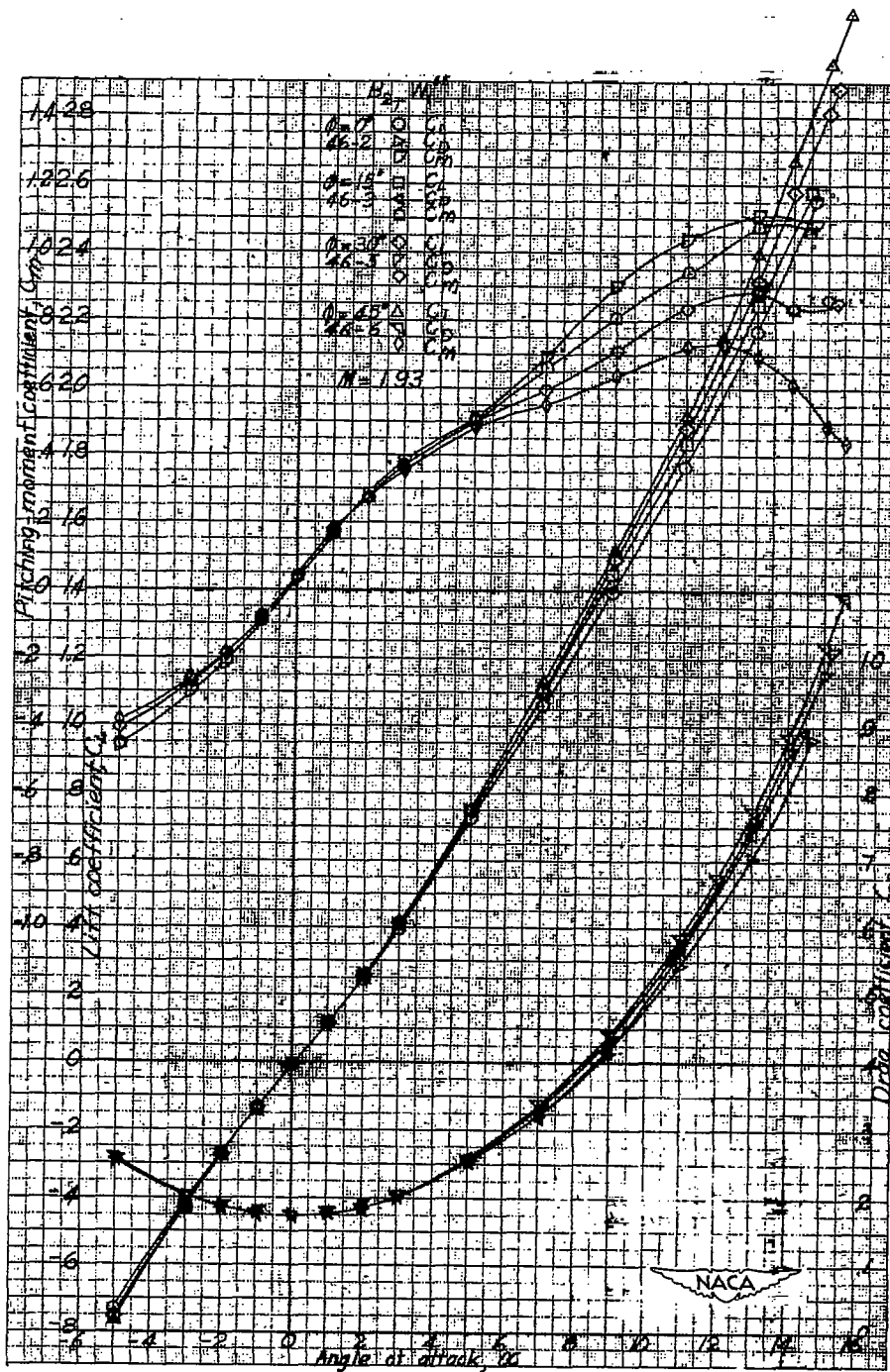


Figure 5.- $M = 1.93$: W_1^{45} increments on B_{2T} at roll angles of 0° , 15° , 30° , and 45° .

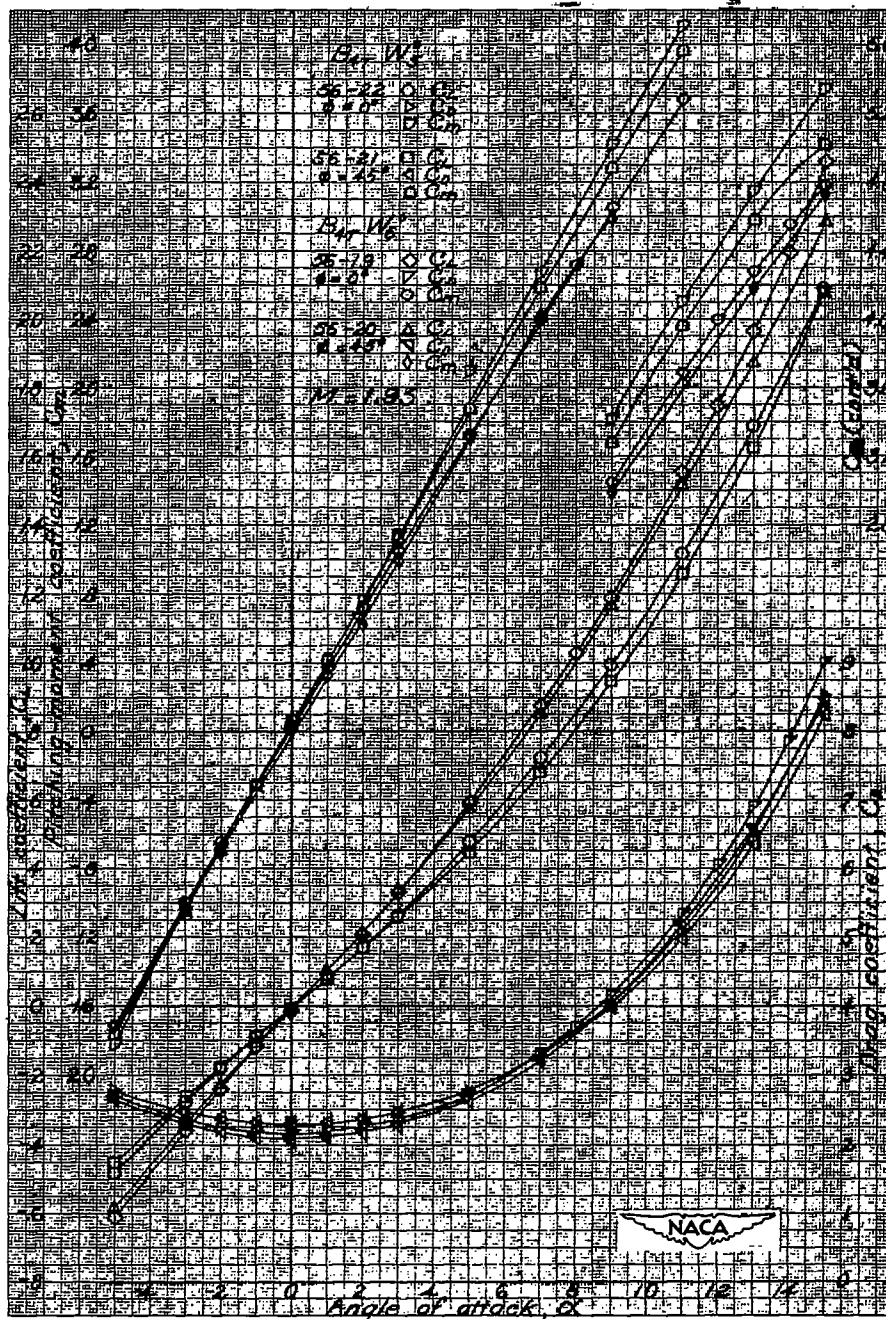


Figure 7.- $M = 1.93$: W_5^0 and W_6^0 increments on B_{4T} at roll angles of 0° and 45° .

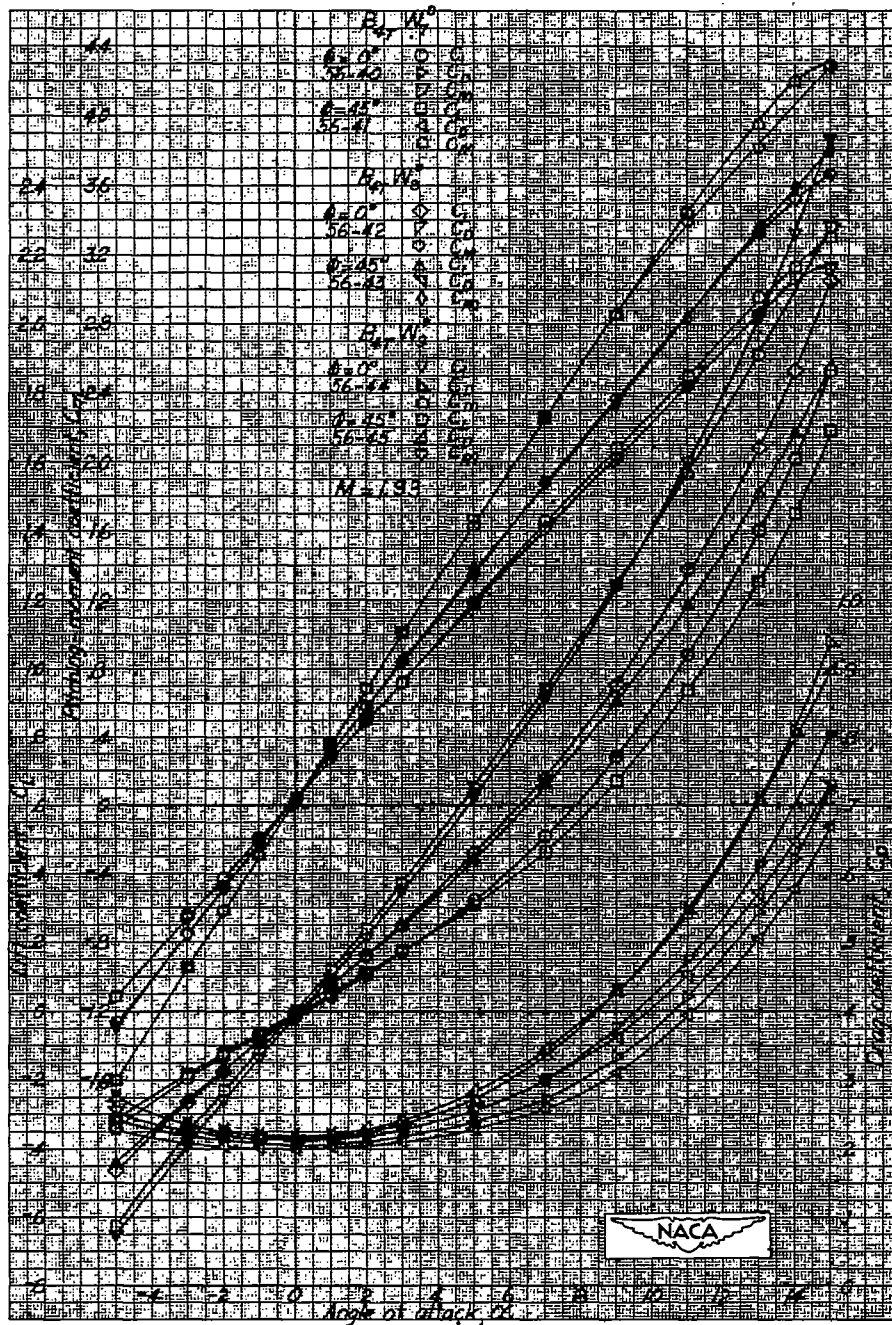


Figure 8.- $M = 1.93$: W_7^0 , W_8^0 , and W_9^0 increments on B_{4T} at roll angles of 0° and 45° .

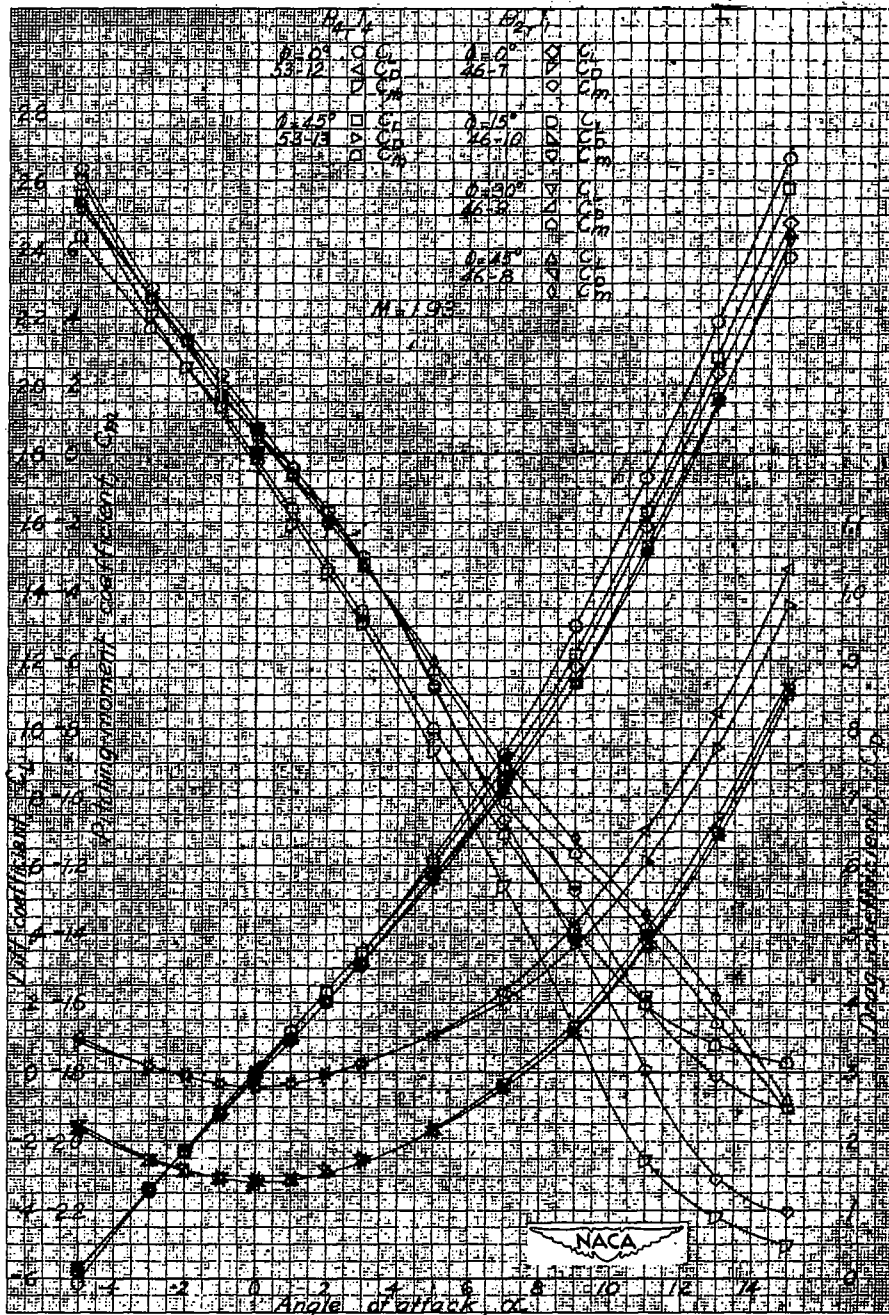


Figure 9.- $M = 1.93$: T_1 increments on B_{2T} at roll angles of 0° , 15° , 30° , and 45° ; T_4 increments on B_{4T} at roll angles of 0° and 45° .

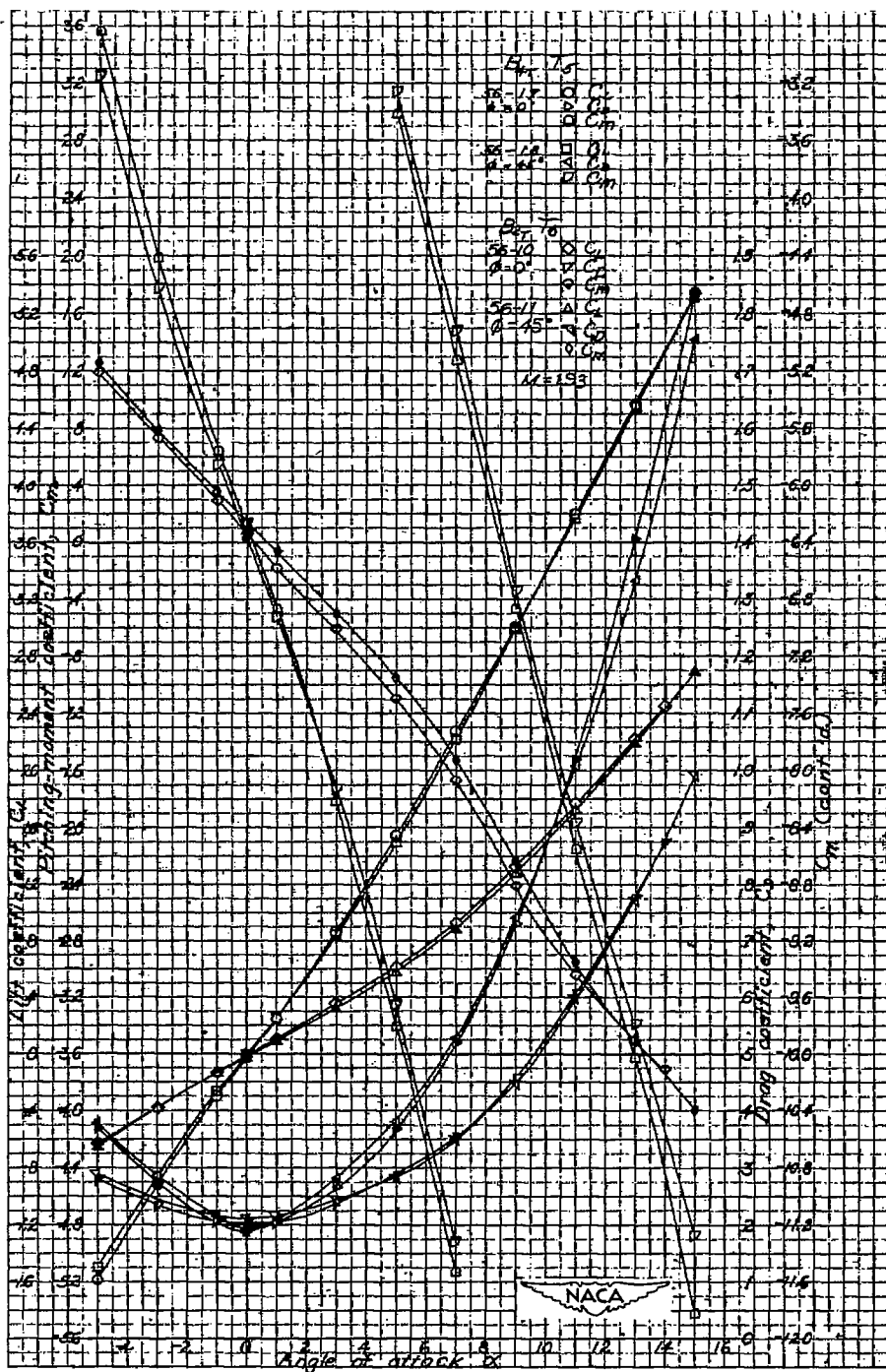


Figure 10.- $M = 1.93$: T_5 increments on B_{14T} at roll angles of 0° and 45° ;
 T_6 increments on B_{2T} at roll angles of 0° and 45° .

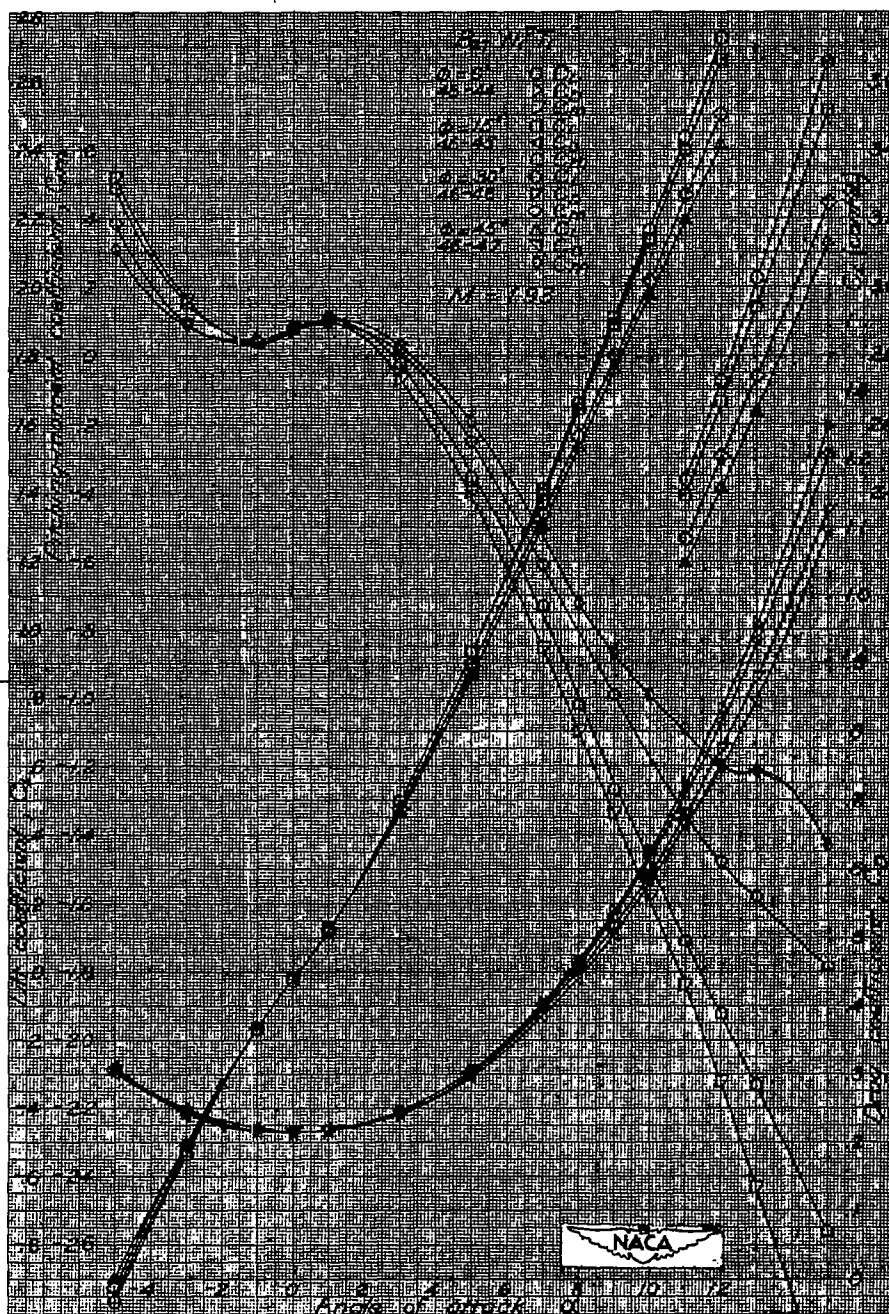


Figure 11.- $M = 1.93$: Effects of roll position on $B_{2T} W_1^0 T_1$; $\phi = 0^\circ, 15^\circ, 30^\circ$, and 45° .

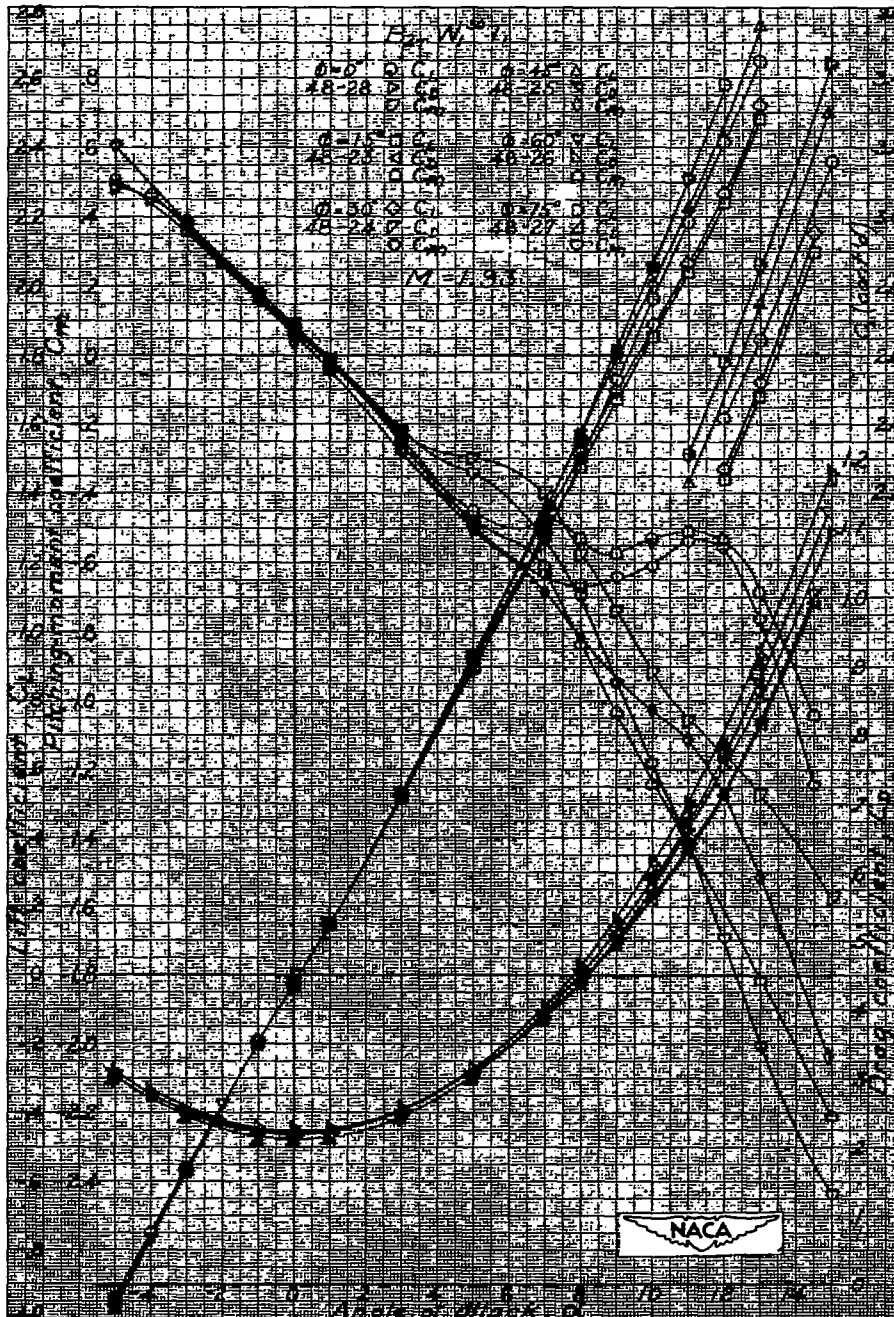


Figure 12.- $M = 1.93$: Effects of roll position on $B_{2T} W_{1T}^{30}$; $\phi = 0^\circ, 15^\circ, 30^\circ, 45^\circ, 60^\circ, \text{ and } 75^\circ$.

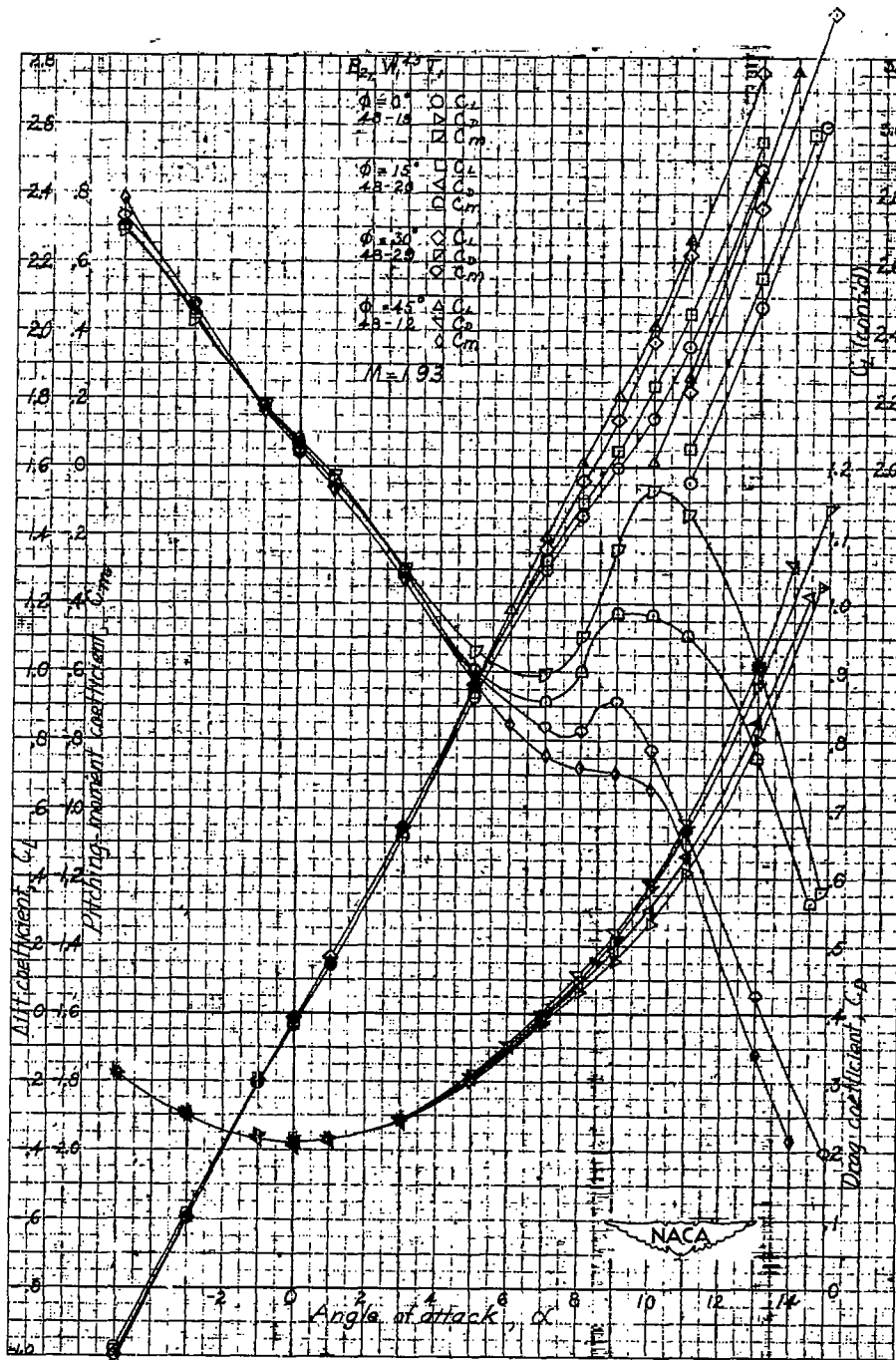


Figure 13.- $M = 1.93$: Effects of roll position on $B_{2T} W_1^{45} T_1$; $\phi = 0^\circ$, 15° , 30° , and 45° .

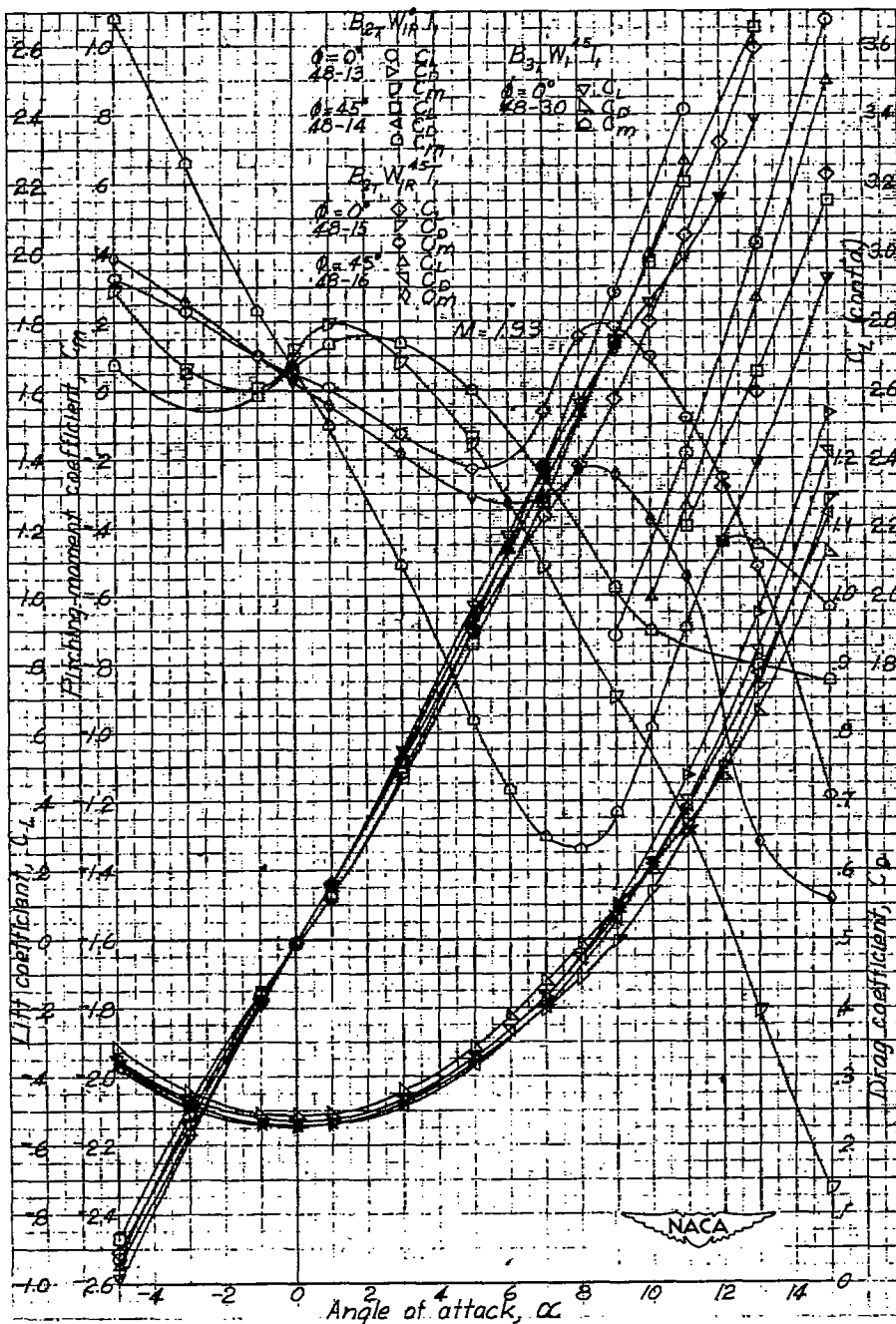


Figure 14.- $M = 1.93$: Effects of roll position on $B_{2T}W_{1R}^0 T_1$ and $B_{2T}W_{1R}^{45} T_1$; $\phi = 0^\circ$ and 45° . Also characteristics of $B_{3T}W_{1R}^{45} T_1$ at $\phi = 0^\circ$.

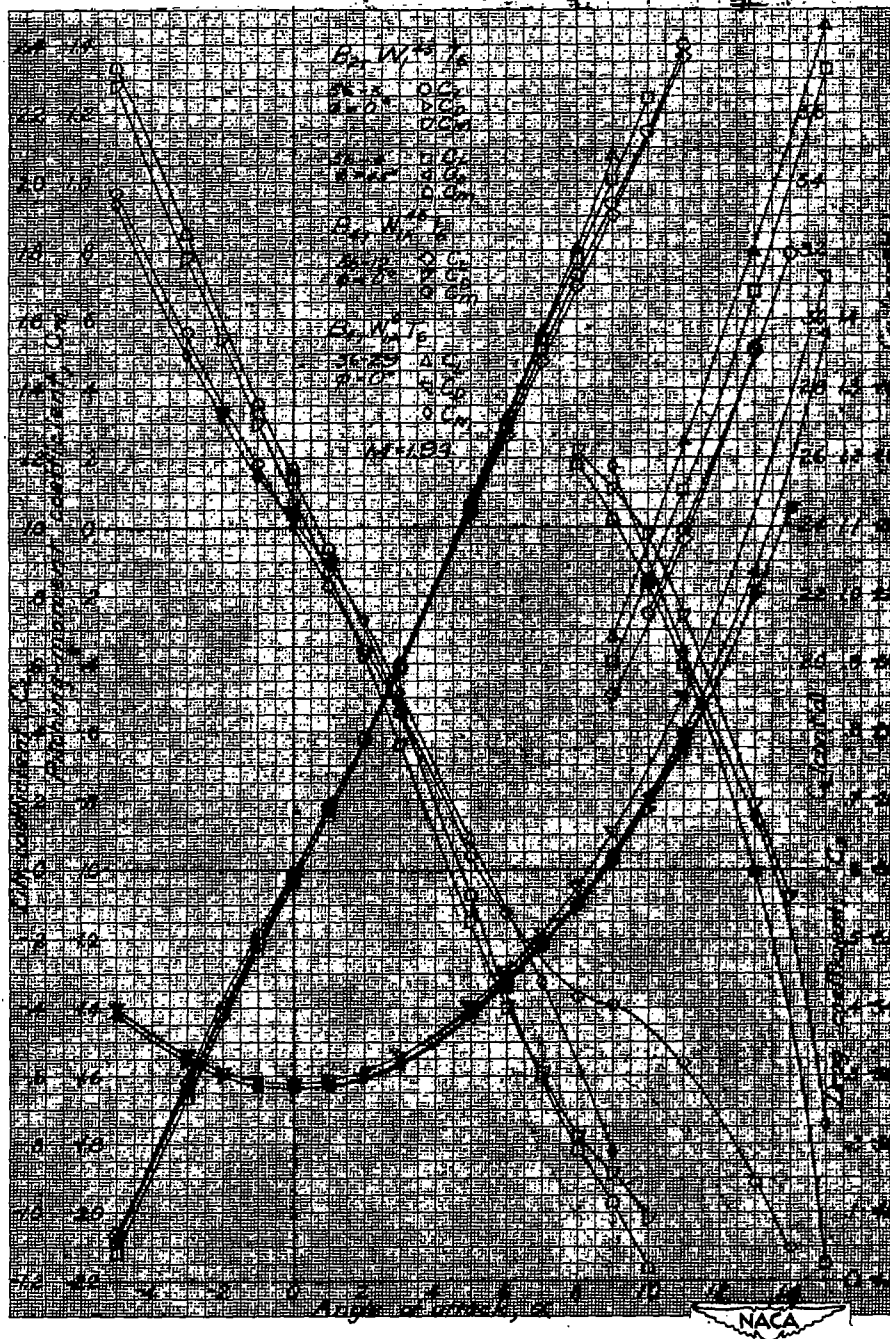


Figure 15.- $M = 1.93$: Effects of roll position on $B_{2T} W_{1T}^{45} T_6$; $\phi = 0^\circ$ and 45° ; also, $B_{4T} W_{1A}^{45} T_6$ and $B_{4T} W_{1A}^{-0} T_6$ at $\phi = 0^\circ$.

~~CONFIDENTIAL~~

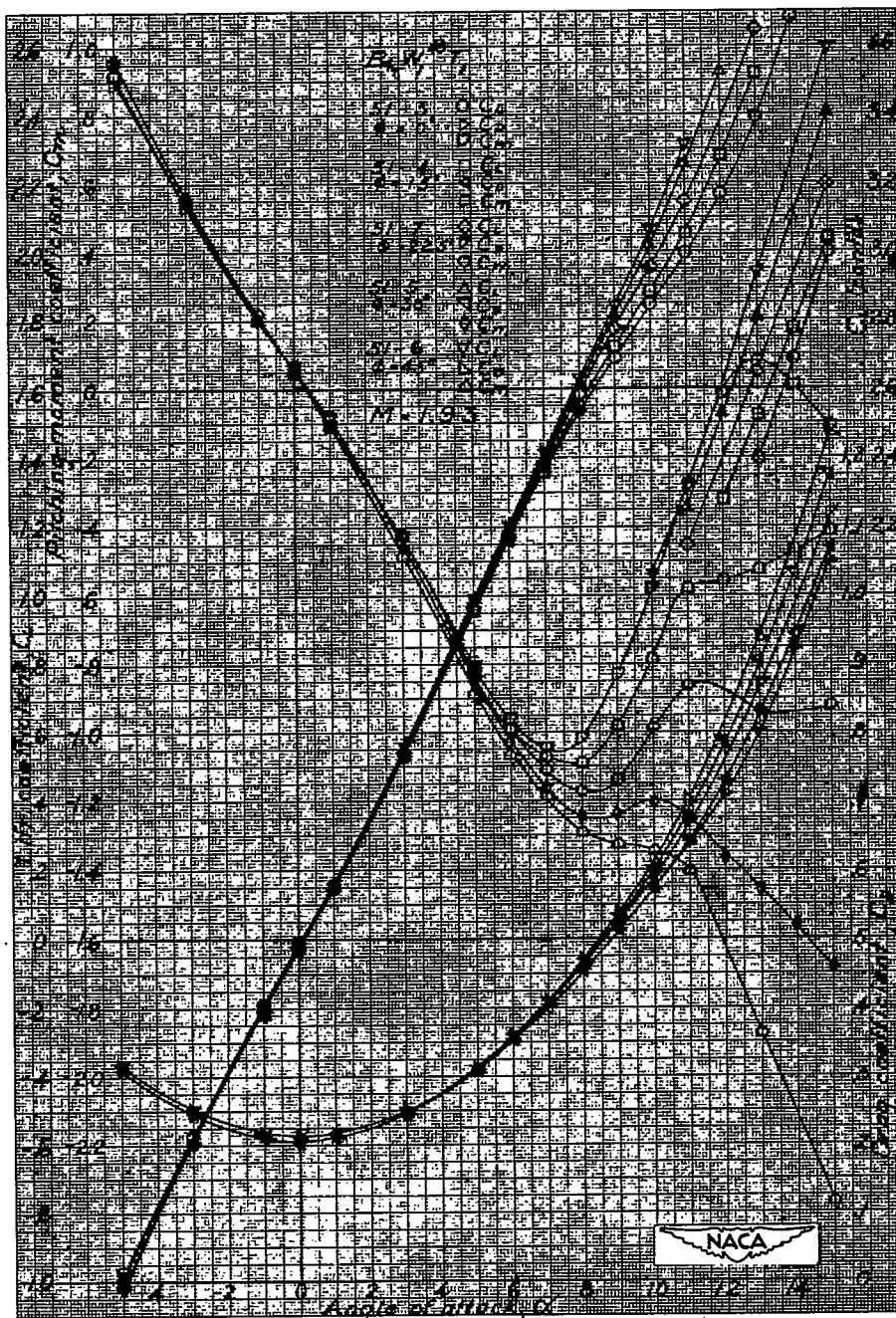


Figure 16.- $M = 1.93$: Effects of roll position on $B_{4T} W_1^{45} T_1$; $\phi = 0^\circ$, 15° , 22.5° , 30° , and 45° .

~~CONFIDENTIAL~~



Figure 17.- M = 1.93: Effects of roll position on $B_{1T} W_{1A}^{45} T_1$ and $B_{1T} W_{1A}^0 T_1$; $\phi = 0^\circ$ and 45° .

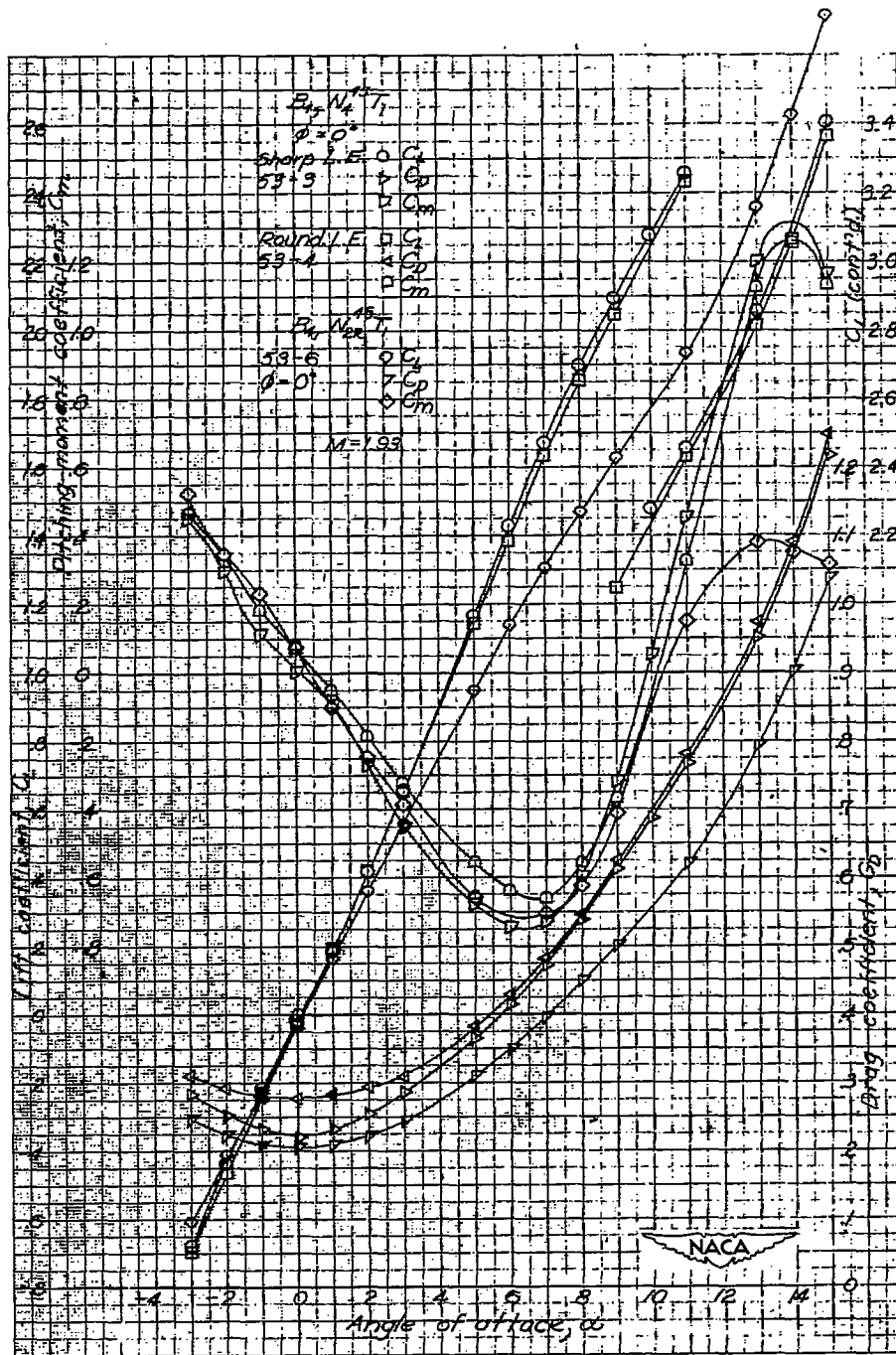


Figure 18.- $M = 1.93$: Characteristics of $B_{4T}W_{2R}^{45}T_1$ at $\phi = 0^\circ$; also, effect of wing leading-edge shape and thickness distribution on $B_{4T}W_4^{45}T_1$ at $\phi = 0^\circ$.

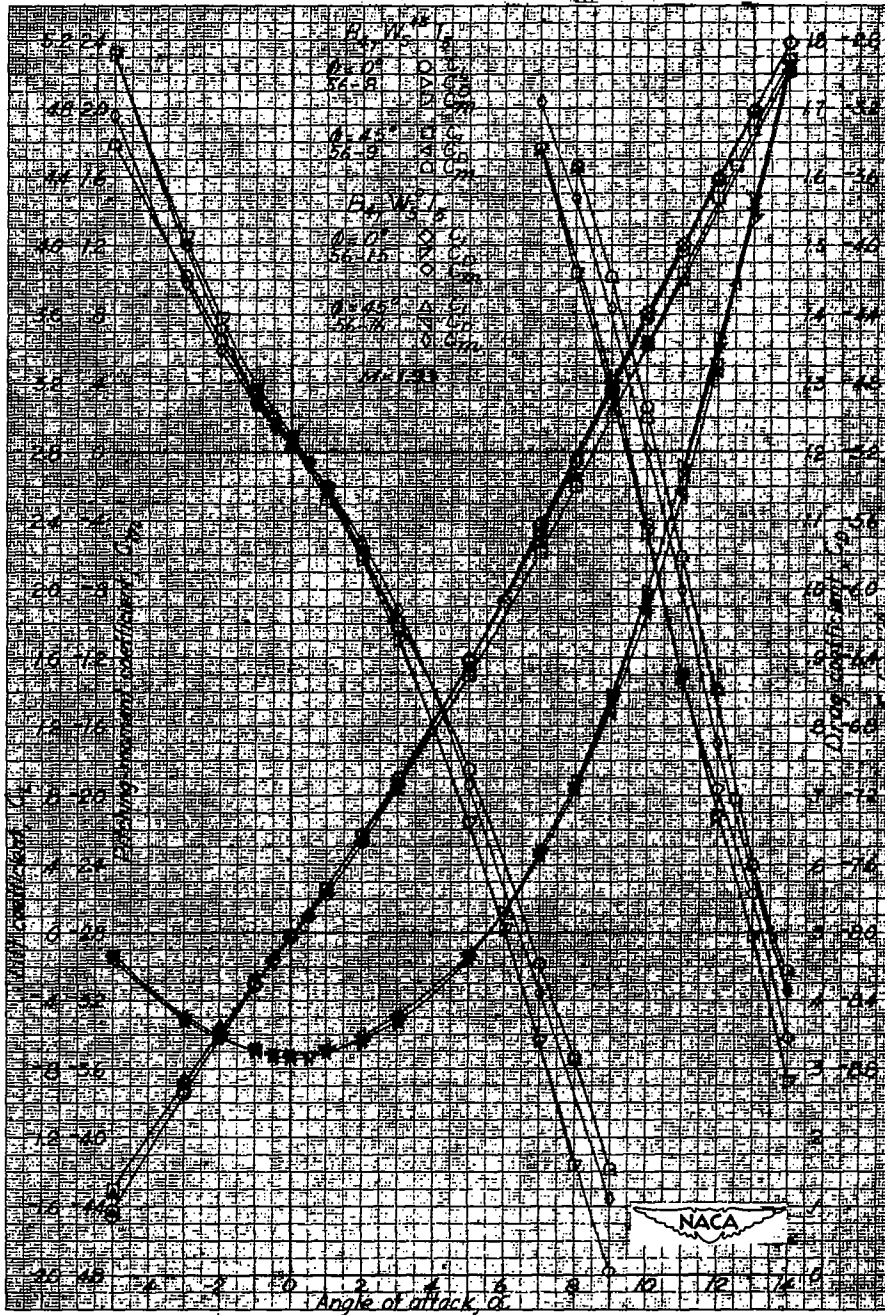


Figure 19.- $M = 1.93$: Effects of roll position on $B_{4T}W_5^{45}T_5$ and $B_{4T}W_5^0T_5$; $\phi = 0^\circ$ and 45° .



Figure 20.- $M = 1.93$: Effects of roll position on $B_{4T}W_6^{45}T_5$ and $B_{4T}W_6^0T_5$; $\phi = 0^\circ$ and 45° .

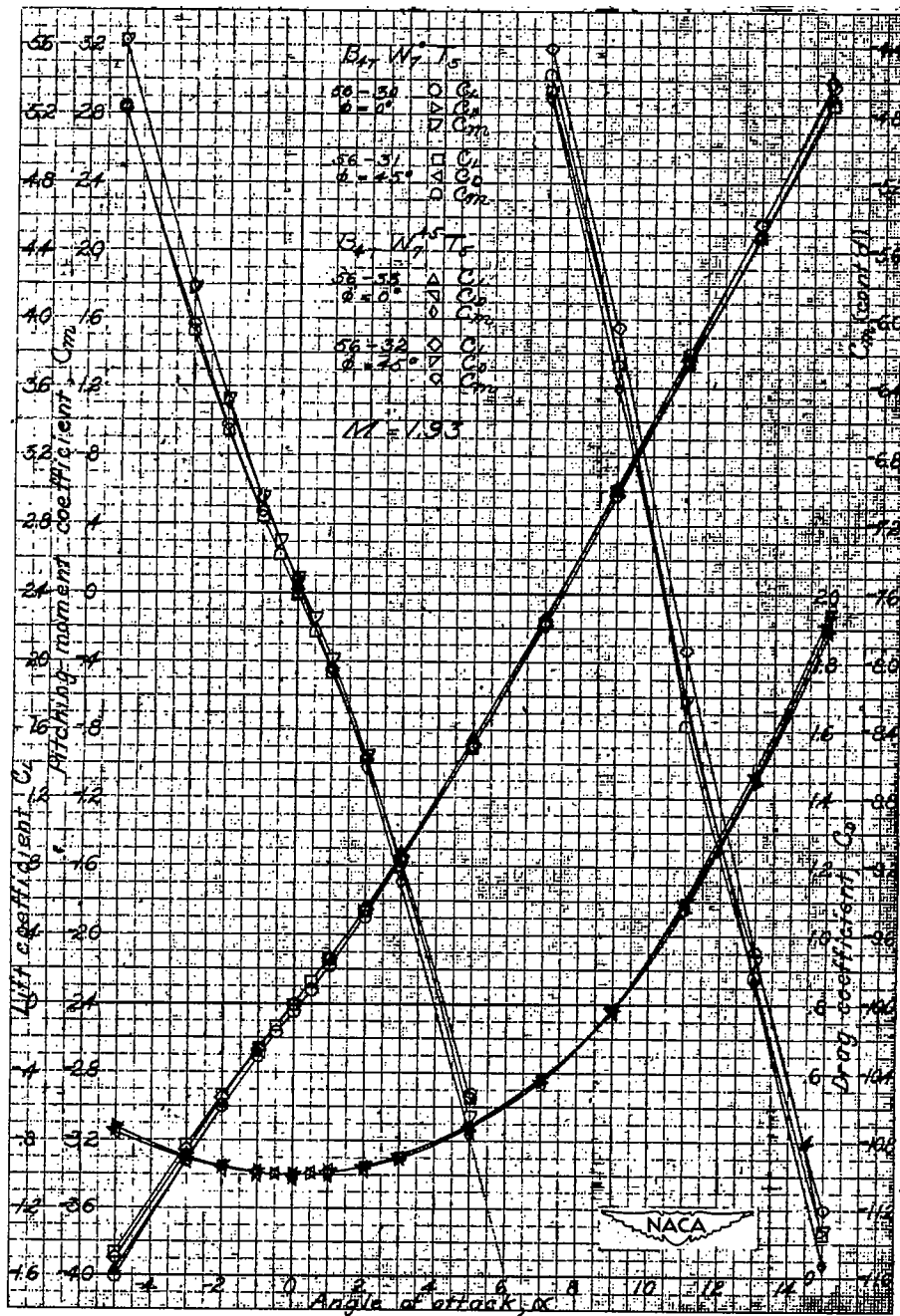


Figure 21.- $M = 1.93$: Effects of roll position on $B_{4T} W_7^{45} T_5$ and $B_{4T} W_7^0 T_5$; $\phi = 0^\circ$ and 45° .

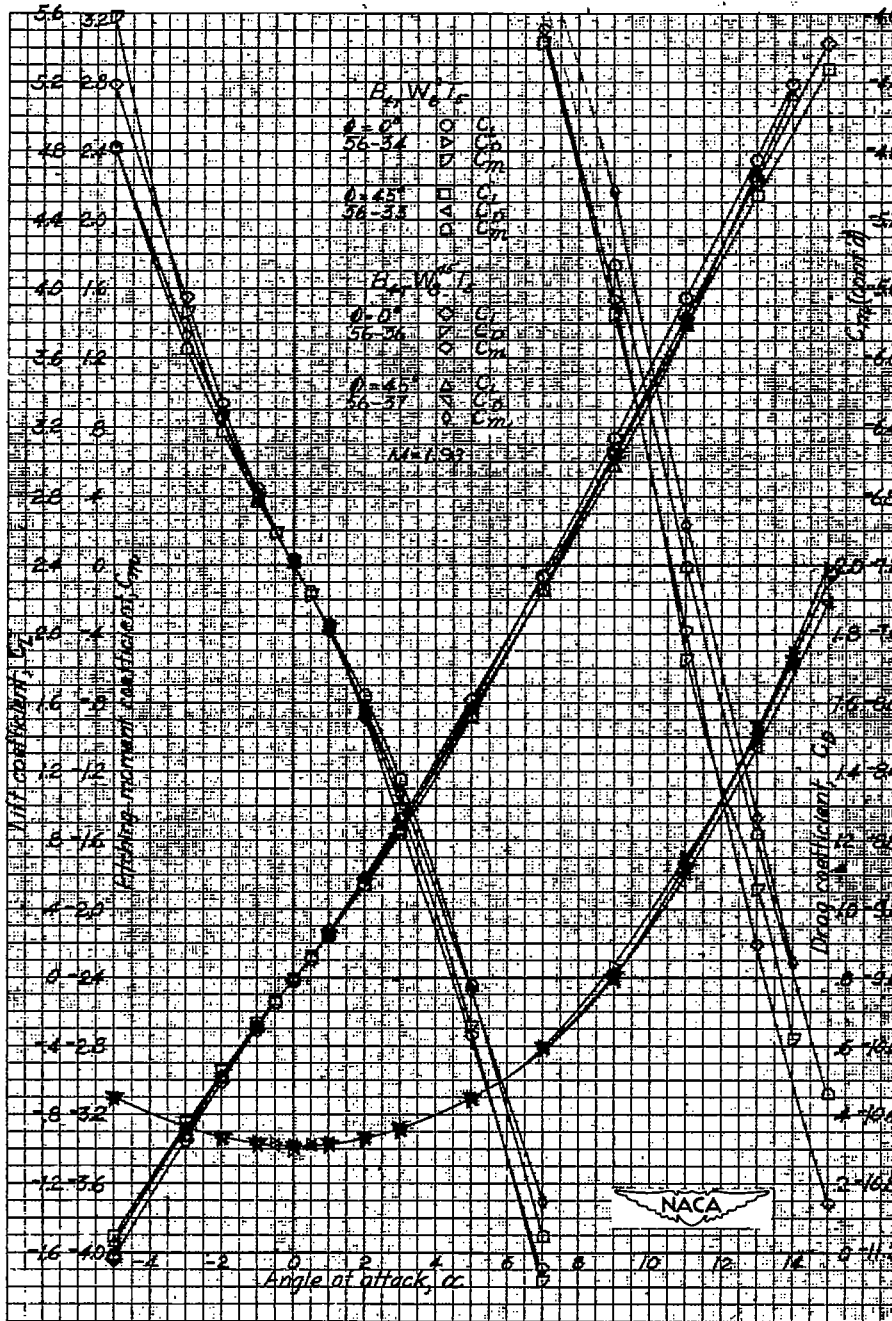


Figure 22.- $M = 1.93$: Effects of roll position on $B_{L_T} W_8^{45T_5}$ and $B_{L_T} W_8^{0T_5}$; $\phi = 0^\circ$ and 45° .

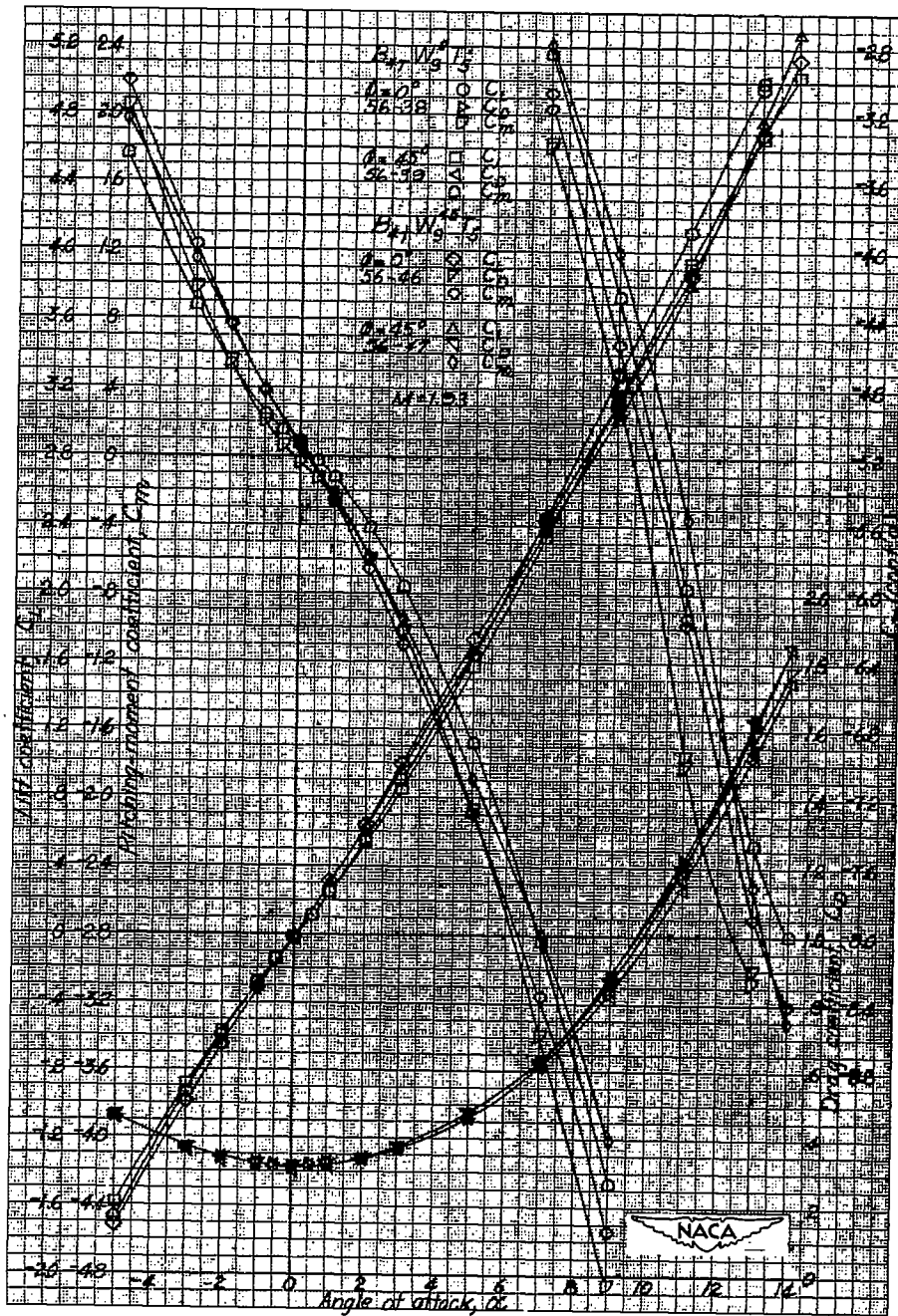


Figure 23.- $M = 1.93$: Effects of roll position on $B_{4T}W_9^{45}T_5$ and $B_{4T}W_9^{0}T_5$; $\phi = 0^\circ$ and 45° .

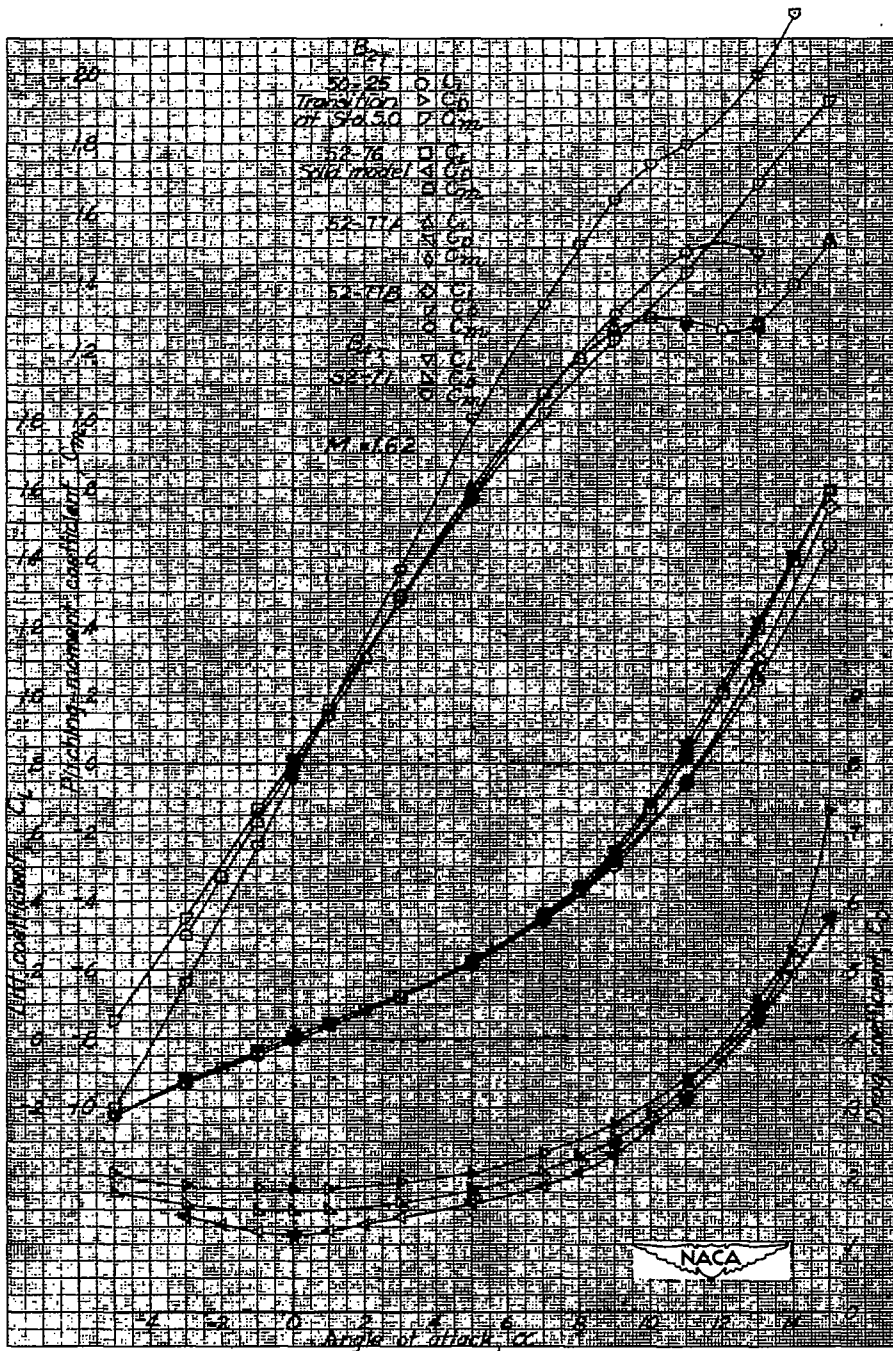


Figure 24.- $M = 1.62$: Basic sectional and solid body characteristics B_{2T} ; effects of transition and misaligned body section on B_{2T} ; also, basic sectional body characteristics of B_{4T} .

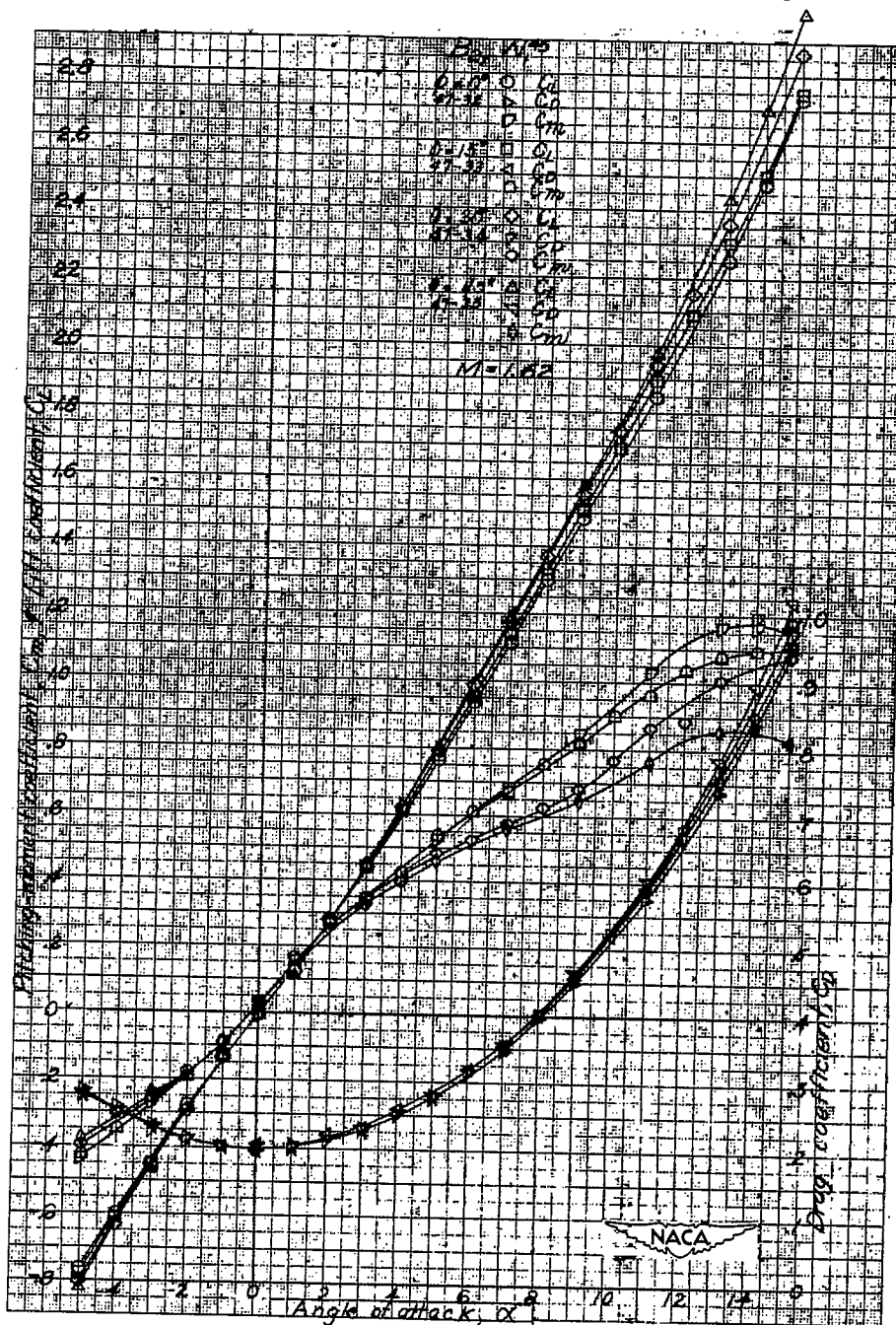


Figure 25.- $M = 1.62$: W_1^{45} increments on B_{2T} at roll angles of 0° , 15° , 30° , and 45° .

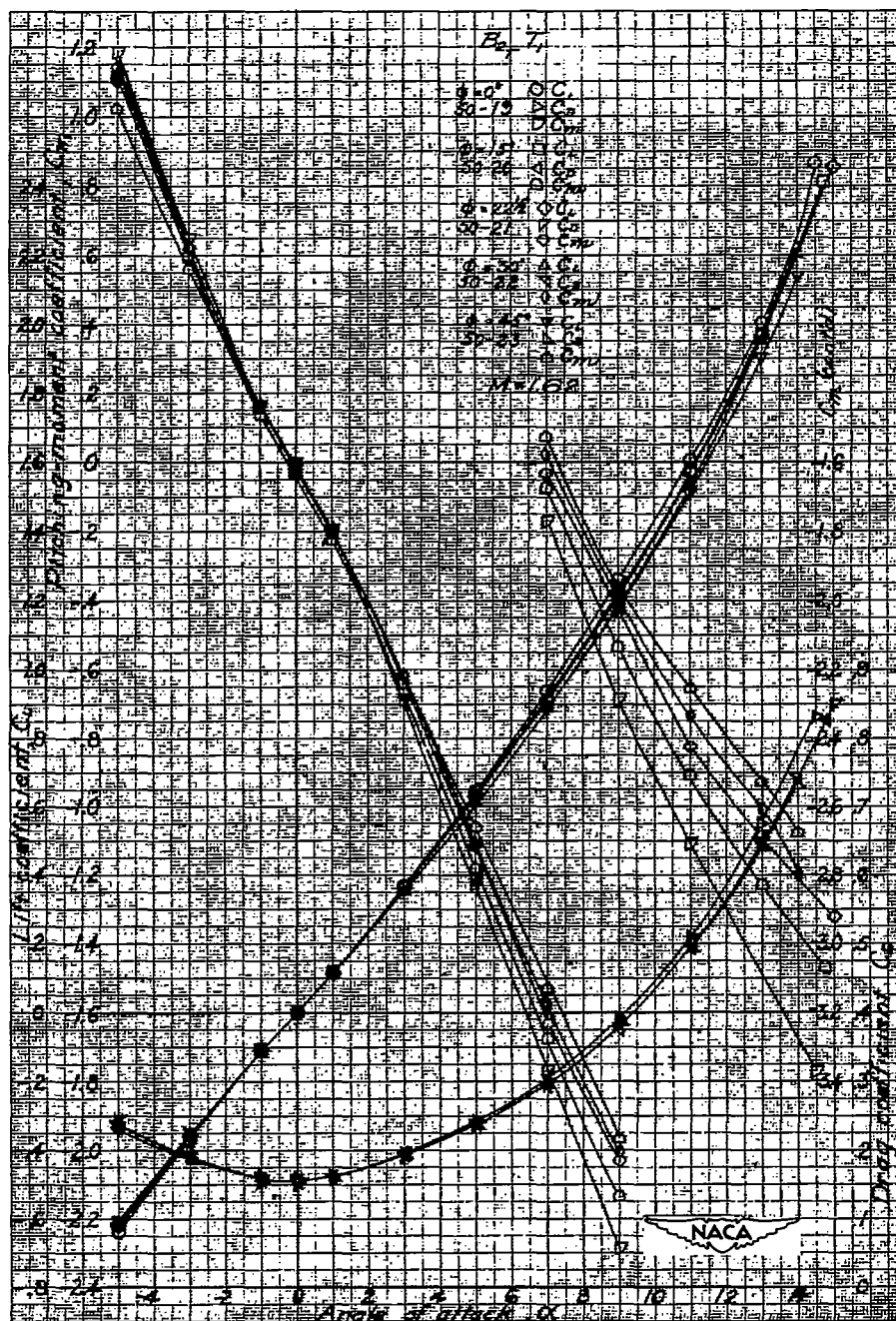


Figure 26.- $M = 1.62$: T_1 increments on B_{2T} at roll angles of 0° , 15° , 30° , and 45° .

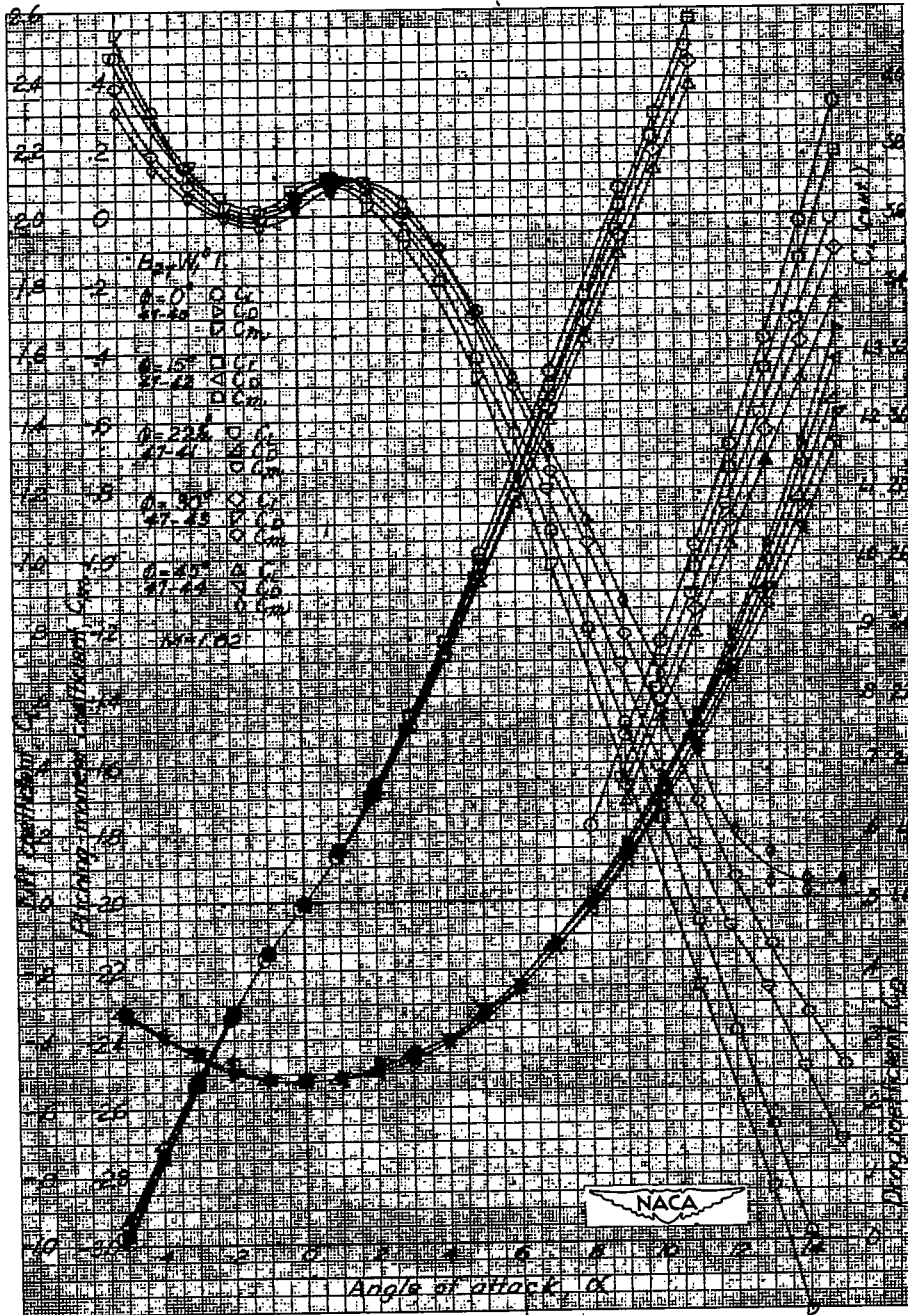


Figure 28.- $M = 1.62$: Effects of roll position on $B_{2T1} W_{1T1}$; $\phi = 0^\circ, 15^\circ, 22.5^\circ, 30^\circ, \text{ and } 45^\circ$.



Figure 29.- $M = 1.62$: Effects of roll position on $B_2 W_1^{30} T_1$; $\phi = 0^\circ$, 15° , 30° , and 45° .

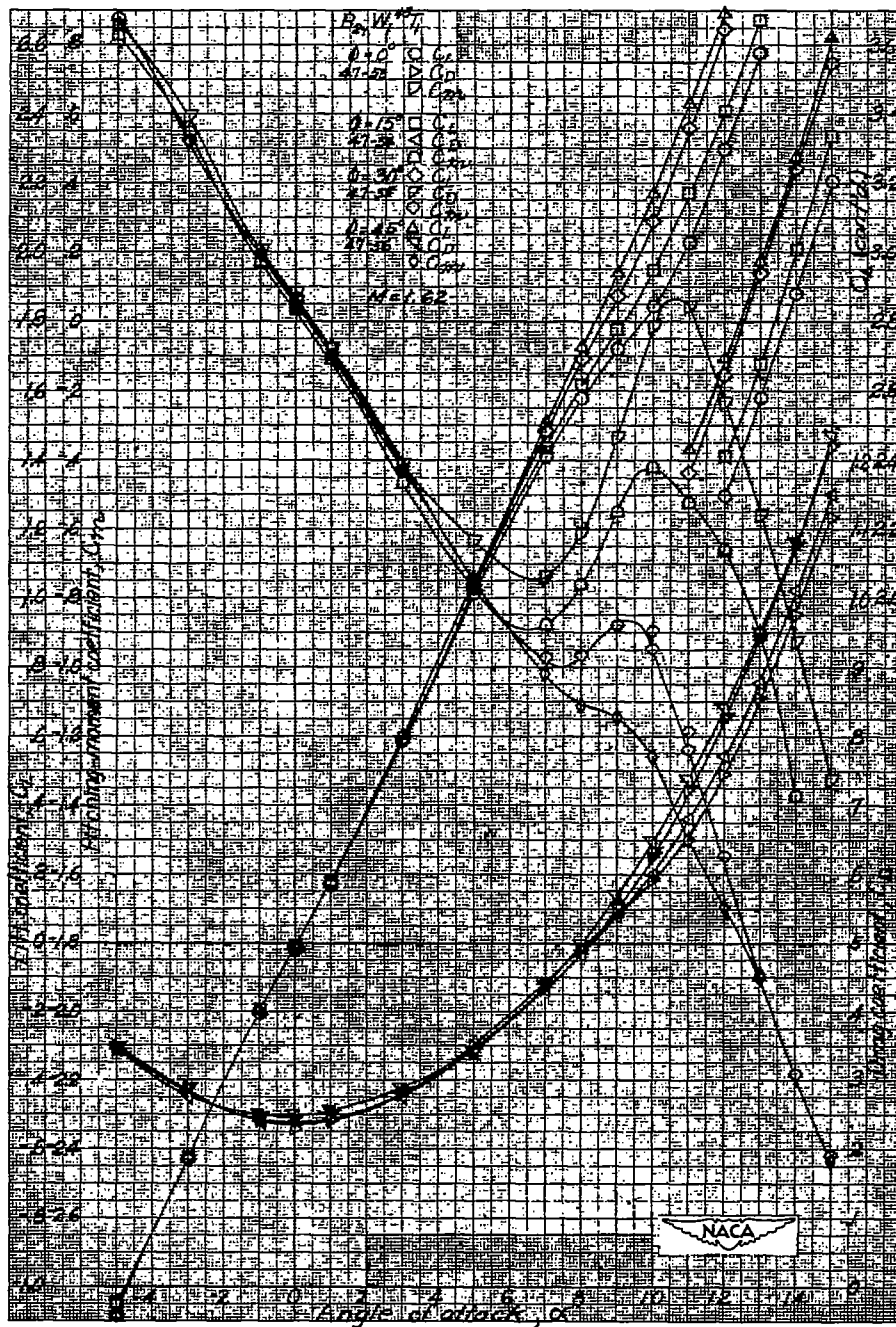


Figure 30.- $M = 1.62$: Effects of roll position on $B_{2T} W_1^{45} T_1$; $\phi = 0^\circ, 15^\circ, 30^\circ, \text{ and } 45^\circ$.

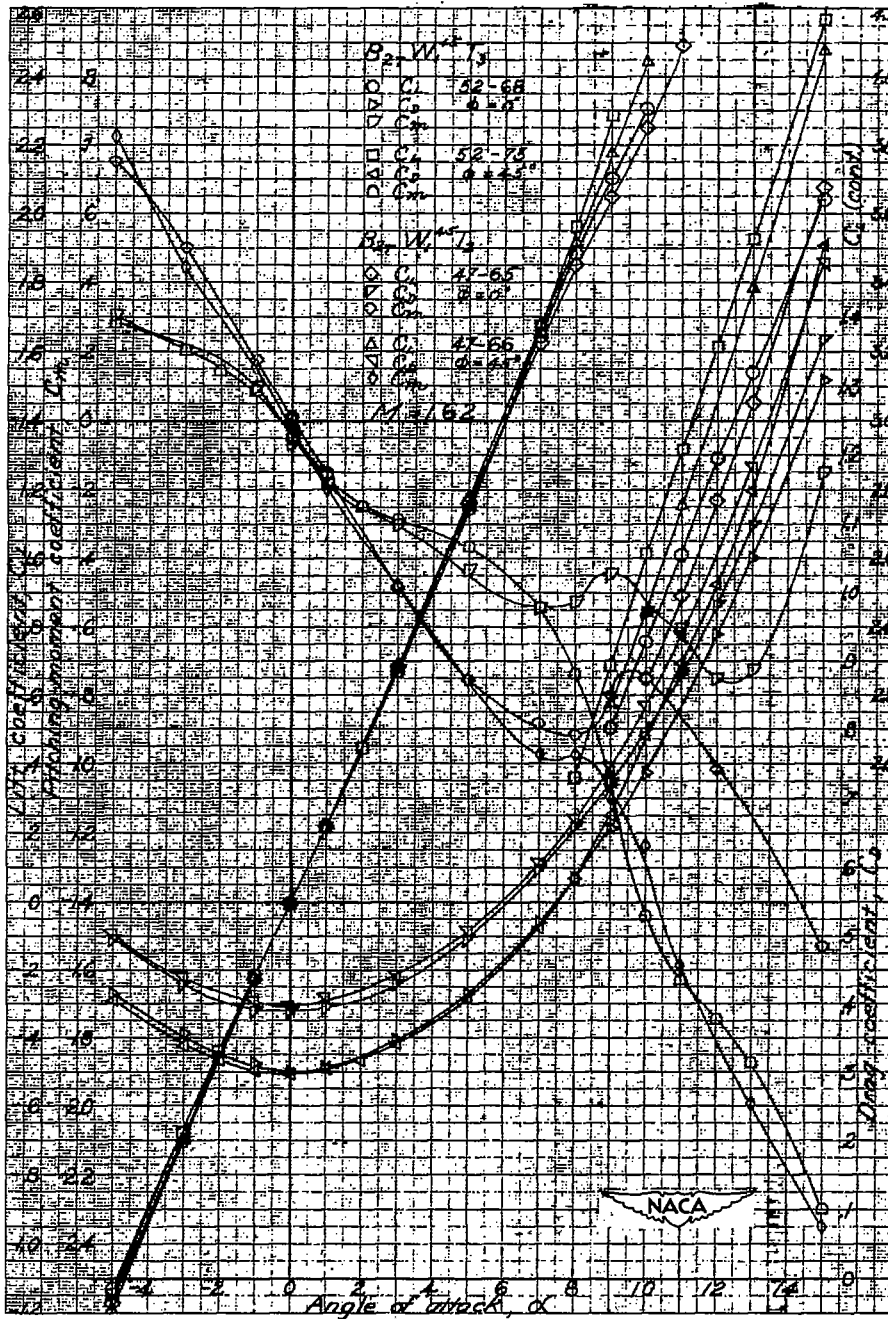


Figure 31.- $M = 1.62$: Comparison of characteristics of $B_{2T}W_1^{45}T_2$ and $B_{2T}W_1^{45}T_3$ at roll angles of 0° and 45° .

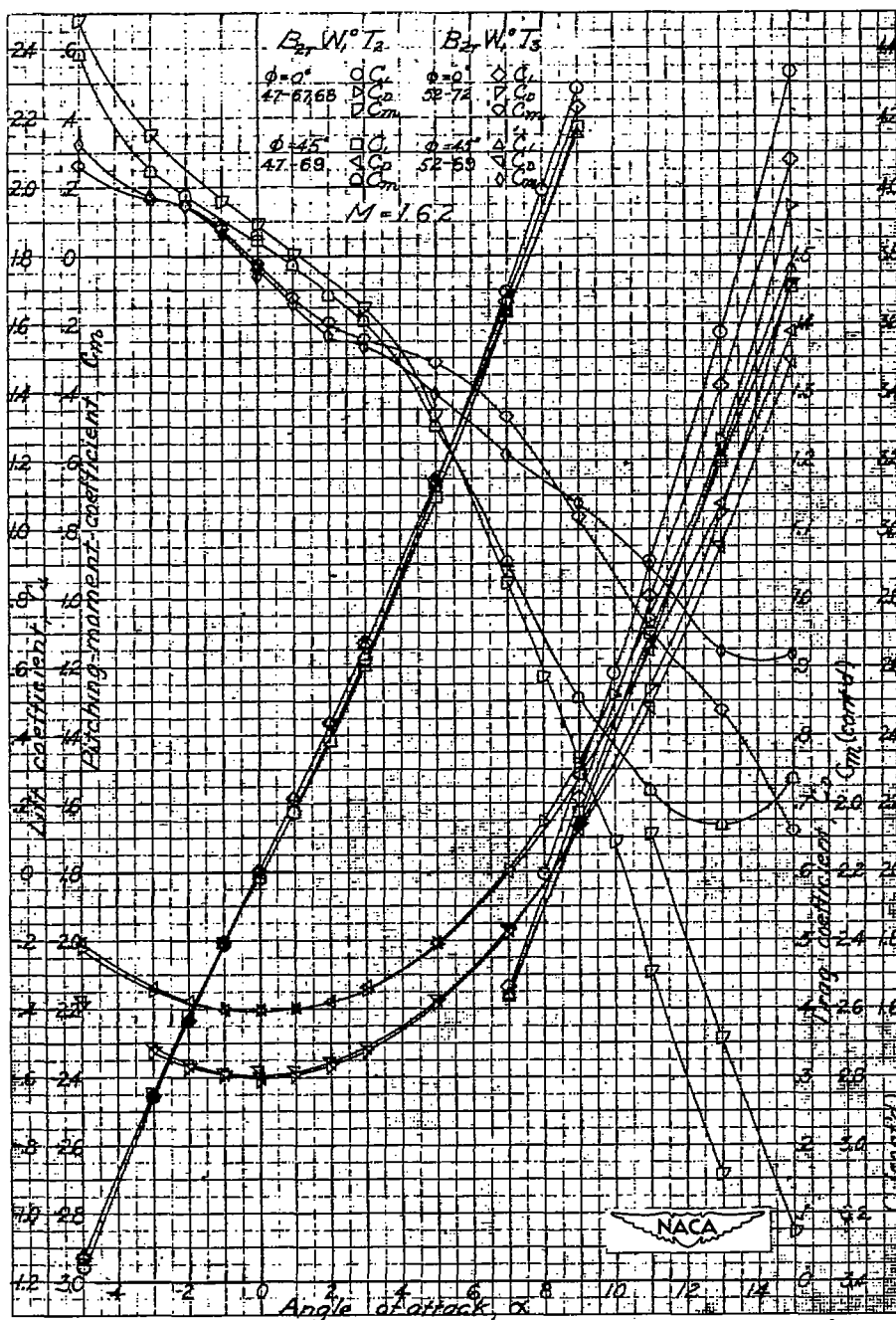


Figure 32.- $M = 1.62$: Comparison of characteristics of $B_{2T}W_1^0T_2$ and $B_{2T}W_1^0T_3$ at roll angles of 0° and 45° .

~~CONFIDENTIAL~~

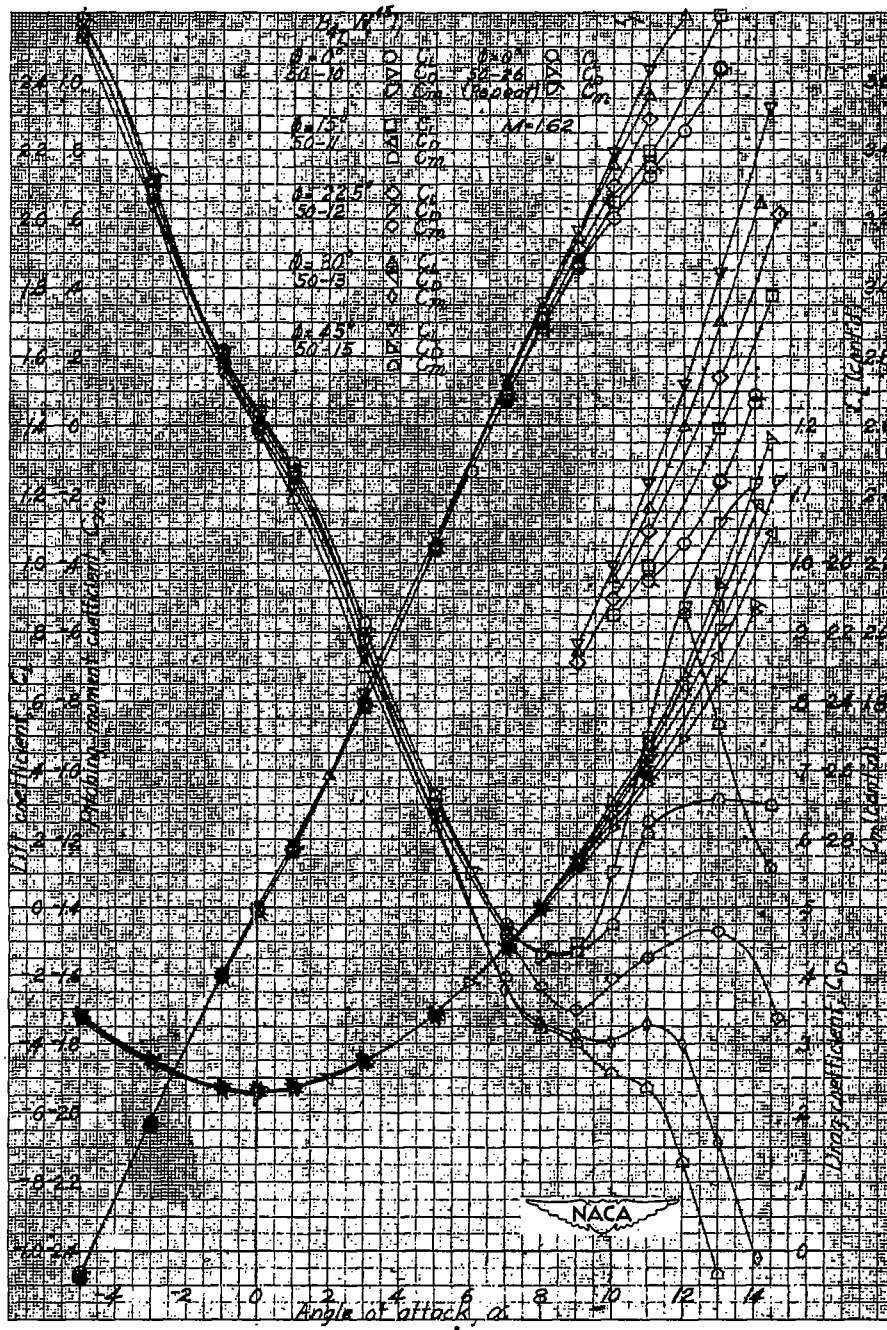


Figure 33.- $M = 1.62$: Effects of roll position on $B_{L_T} W_{T_1}^{45}$; $\phi = 0^\circ$, 15° , 30° , and 45° .

~~CONFIDENTIAL~~

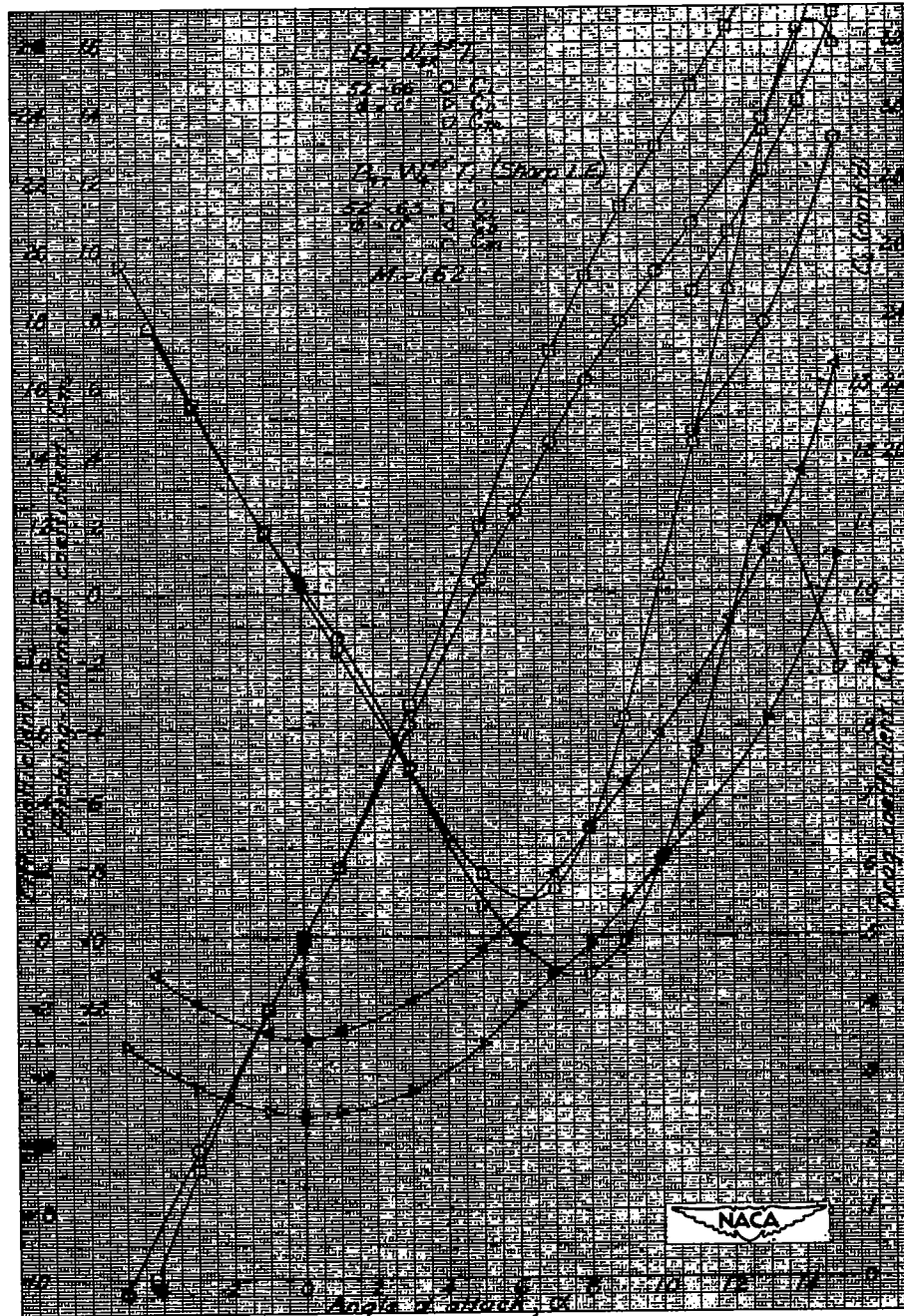


Figure 34.- M = 1.62: Characteristics of $B_{4T}W_{2R}^{45T_1}$ and $B_{4T}W_4^{45T_1}$ (with sharp leading edge) at $\phi = 0^\circ$.

~~CONFIDENTIAL~~

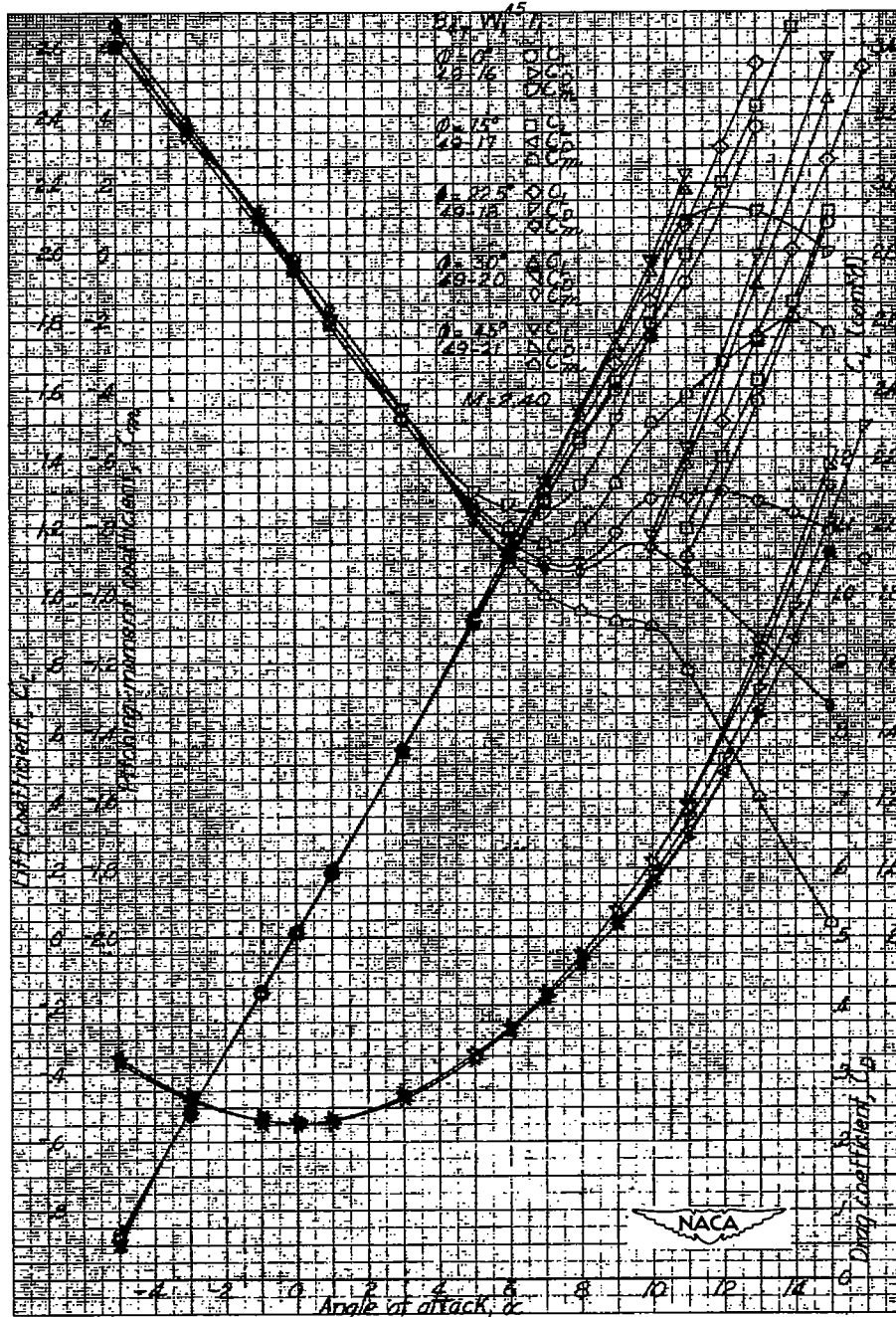


Figure 36.- $M = 2.40$: Effects of roll position on $B_{4T} W_1^{45} T_1$; $\phi = 0^\circ, 15^\circ, 22.5^\circ, 30^\circ, \text{ and } 45^\circ$.

~~CONFIDENTIAL~~

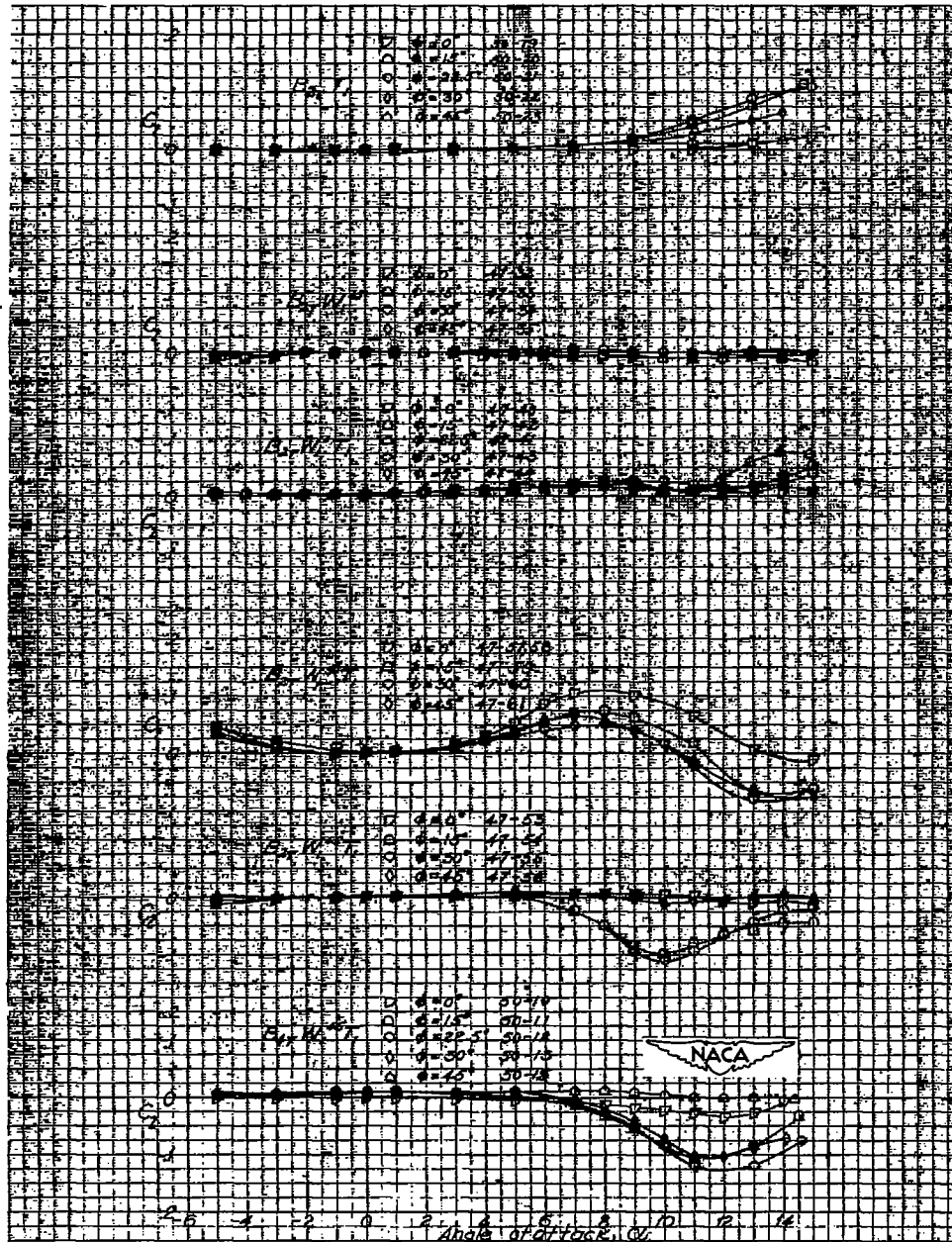


Figure 38.- $M = 1.62$: Rolling-moment characteristics of various configurations.

~~CONFIDENTIAL~~

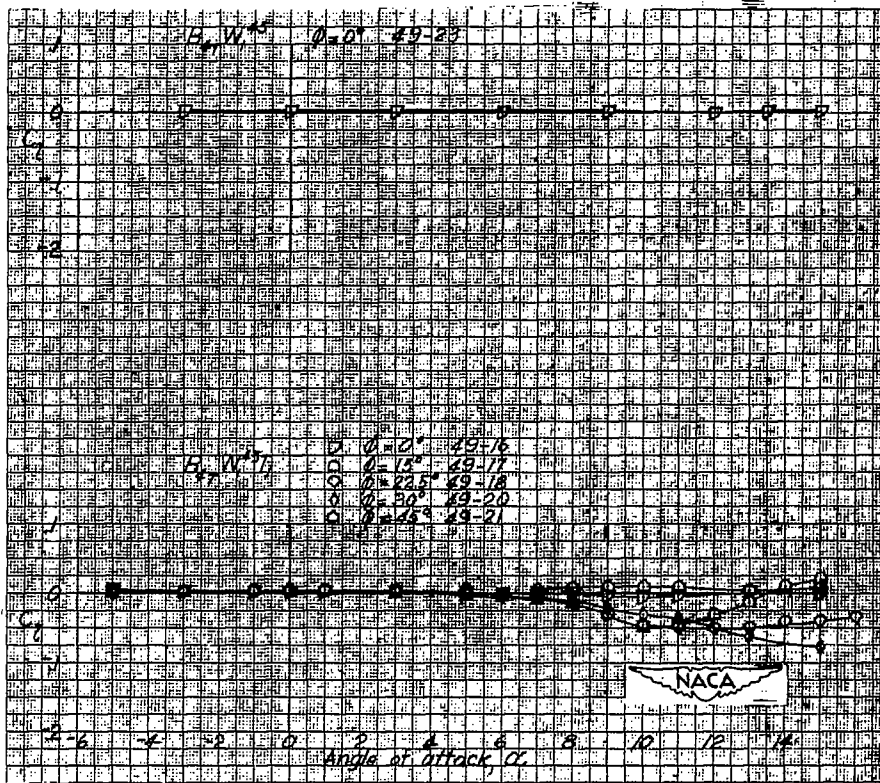


Figure 39.- M = 2.40: Rolling-moment characteristics of various configurations.

~~CONFIDENTIAL~~